TÉCNICO LISBOA

White holes

Formation and dynamics

Vasco Luís Ribeiro Récio Pires

Thesis to obtain the Master of Science Degree in

Engineering Physics

Supervisors:
Prof. Vitor Manuel dos Santos Cardoso
Prof. José António Maciel Natário

Examination Committee

Chairperson: Prof. Ilídio Pereira Lopes
Supervisor: Prof. Vitor Manuel dos Santos Cardoso
Member of the Committee: Prof. Richard Pires Brito

November 2025

Declaration

I declare that this document is an original work of my own authorship and that it fulfills all the requirements of the Code of Conduct and Good Practices of the Universidade de Lisboa.

To the memory of Eugénio Récio

Acknowledgments

I must start by expressing my gratitude to my supervisors, Vitor Cardoso and José Natário, for their guidance and lessons in physics, research, and indirectly in life. Thank you immensely for your patience and help with my mistakes throughout this thesis. Learning from such talented and incredible researchers has been a truly honourable experience, from knowledge to work habits and physics discussions, it was an enriching and of unmeasurable value opportunity that I will take for the rest of my life. Thank you for the support, encouragement and insight for the next steps of my academic life.

To my mother, Fátima, for being such a bright and strong light in my life, an example of a hard working and wonderful person who has given me unconditional support and love on this journey. I cannot put into words all that you did for me, I love you mom, I hope I can give it back to you and more. To my father, Luís, who very early gave me the basis of responsibility and determination that I will take for life. Thank you for all your encouragement, lessons, and fun weekend mornings. I love you dad, I hope things get better. To all of my family for their support and encouragement, I prefer not to name you all in the risk of forgetting someone. Nonetheless, I must express special gratitude towards my grandparents, Eugénio, Júlia, José and Ana for taking care of me in these years and transmitting crucial values that I will carry throughout life. And also my uncle, João, who showed me how I can always look at the bright side of life, I love you all.

To my girlfriend Carolina, for all the love and happiness you brought to my life in these years. Thank you for all your support, encouragement and for believing in me, even when it was difficult for me to do so. Your bright soul and your great advice inspire me to be better every day. Vienna waits for us.

I would like to thank ”Os putos estúpidos”: Paula, Joni, João and Carolina, one of the best things Técnico brought into my life. It has been truly an honour and a pleasure to be on this journey with you. From all the uncountable incredible experiences, laughs, tears, life threatening moments and unconditional support that we shared, thank you so much, from the bottom of my heart, for being part of my life. A special thanks to Paula and Joni for taking me under their wings in those early difficult days.

To the rest of my chosen family, Tiago, Gil and Matilde, thank you for all your support, guidance, inspiration, and love. This journey from high school to now has been a roller-coaster, but you were always there for me, showing that I was never alone and shaping me into the person I am today. Thank

you for all those hangouts, late night dinners, car talks, trips, laughs, and talking about my physics passions and theories. To all my friends, I will always carry you in my heart.

I also wish to thank my rugby club ”Grupo Desportivo Direito”, coaches and mates who brought me wonderful and important values, work ethics, and life lessons that I will keep close to my core.

Abstract

Einstein's theory of General Relativity allows for the possibility of the existence of remarkable and exotic macroscopic objects. Two examples are black holes and white holes. For the first, the evidence for their existence is overwhelming, and their properties have been studied in detail. White holes, on the other hand, have not received as much attention, and their existence is still an open question.

Although we have not had any confirmed detections, white holes are still solutions to Einstein's equations. These are truly strange objects that defy our physics, but so do black holes up to this day. That is why further study of the formation and dynamics of these objects is necessary. A better understanding may reveal important implications for black hole physics and cosmology, which can change our understanding of the universe.

In this thesis, we analyse a model for a white hole originating from an inverted Oppenheimmer-Snyder collapse. We study the possible solutions of this model, depending on the initial conditions. In addition, we study the dynamics of the white hole, with a first approach through the quasinormal modes. Finally, to compare our results with the state-of-the-art work, we review the more recent literature addressing quasinormal modes of a Schwarzschild white hole.

Keywords

White Holes; Black Holes; Matching; Carter-Penrose diagrams; Quasinormal modes.

Resumo

A teoria da Relatividade Geral de Einstein permite a existência de objetos macroscópicos notáveis e exóticos. Dois exemplos são os buracos negros e os buracos brancos. No primeiro caso, as evidências da sua existência são abundantes e as suas propriedades foram estudadas em detalhe. Os buracos brancos, por outro lado, não receberam tanta atenção, e a sua existência ainda é uma questão em aberto.

Embora não haja uma detecção confirmada, os buracos brancos ainda são soluções das equações de Einstein. São objetos realmente estranhos que desafiam a nossa física, mas o mesmo acontece com os buracos negros até hoje. É por isso que é necessário continuar a estudar a formação e a dinâmica destes objetos. Uma melhor compreensão pode revelar implicações importantes para a física de buracos negros e para a cosmologia, transformando a nossa compreensão do universo.

Nesta dissertação, analisamos um modelo para um buraco branco que surge de um colapso de Oppenheimmer-Snyder invertido. Estudamos as possíveis soluções deste modelo, dependendo das condições iniciais. Além disso, estudamos a dinâmica do buraco branco, com uma primeira abordagem através dos modos quasinormais. Por fim, de forma a comparar os nossos resultados com a literatura, revemos um dos poucos e mais recentes trabalhos sobre estes modos para um buraco branco em Schwarzschild.

Palavras Chave

Buracos Brancos; Buracos Negros; Colagem; Diagramas de Carter-Penrose; Modos quasinormais;

Contents

List of Figures

List of Tables

Acronyms

WH	white hole
BH	black hole
RN	Reissner-Nordström
FLRW	Friedman-Lemaître-Robertson-Walker
WKB	Wentzel–Kramers–Brillouin
TTMs	total transmission modes
TTM$_L$s	“left”-total transmission modes
TTM$_R$s	“right”-total transmission modes

1

Introduction

Since Karl Schwarzschild discovered the first exact solution of the Einstein equations, the world of cosmology and astrophysics was never the same. Over the years, many important physicists and mathematicians have studied this spacetime, providing enlightenment on this topic, as well as new questions and challenges. They have shown us the possibilities that different black hole spacetimes bring to our universe, enhancing our understanding and knowledge to a different level. It is for me an honour to work on their shoulders and through their work. For all these different black hole spacetimes, going back to Schwarzschild, we are presented with consequences and outcomes that have shocked the world of physics. However, a common trait in all of them, is the fact that there are always two opposite objects present, in both simple and complex solutions. As an example, we present the maximal analytical extension of Schwarzschild, Reissner-Nordström (RN) and Kerr spacetimes.

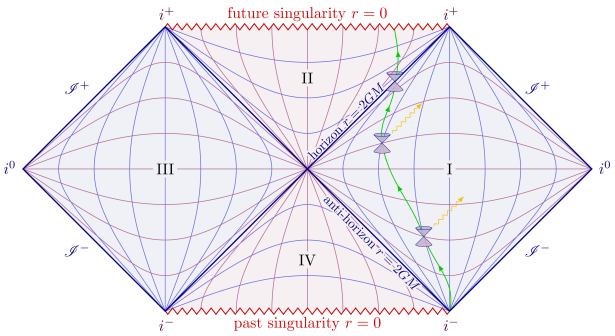

Figure 1.1: Maximal analytical extension of Schwarzschild spacetime [1].

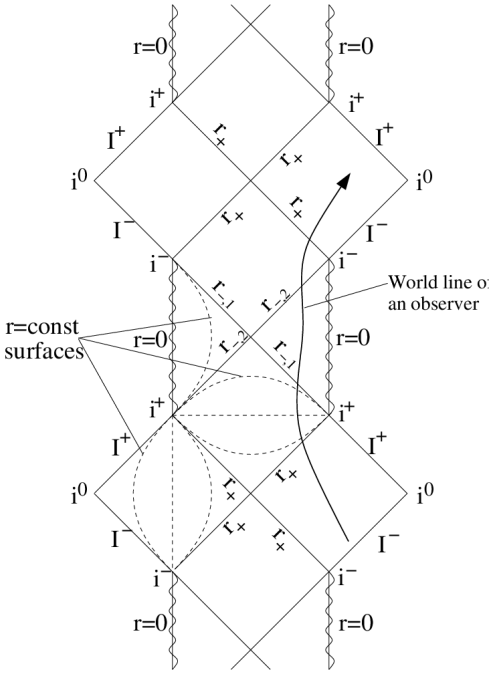

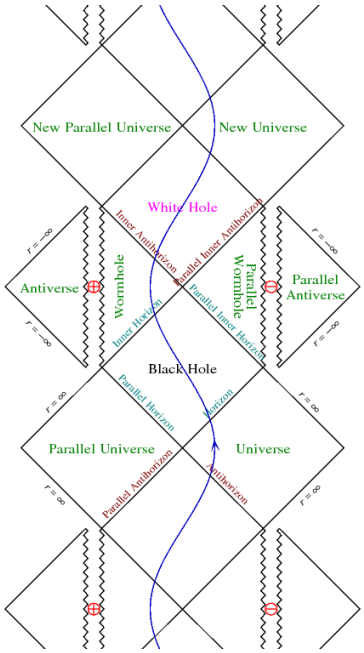

Figure 1.2: Maximal analytical extension of Reissner-Nordström [2] (left) and Kerr [3] (right) spacetimes.

Comparing the last two diagrams with the Schwarzschild one, we see that by simply adding a charge Q for RN, or a spin a for Kerr, the outcomes are radically different. However, despite their differences, it is clear that all diagrams possess future and past singularities. These spacetimes feature two objects that, despite both having a singularity, present opposite properties that make these solutions even more interesting. The more well-known object is the black hole (BH). This astrophysical object is present in some spacetimes possessing in its centre a veiled singularity [4]. Inside the BH, spacetime is so bent that neither matter nor even light can escape past a specific radius called the event horizon. They are one of the simplest objects in our universe, characterised, at their final stages, simply by their mass and, in more complex cases, their spin and/or charge, according to the *no hair theorem* [5]. However, it is worth mentioning that it has become widely accepted that BHs have practically no charge. These are, without a doubt, some of the most exotic and extreme objects in our universe, defying the physics and the laws of the universe. Nonetheless, it is through their darkness that we may find some light.

These objects have been extensively studied over the years, from their formation by Oppenheimer and Snyder [6], to the James Webb Space Telescope exploring other formation possibilities. Phenomena associated with BHs have been uncovered, from Hawking radiation [7] to superradiance [8], a radiation-enhancement process with important implications in searches for dark matter and physics beyond the Standard Model. Quasinormal modes, first discussed by Vishveshwara [9], are characteristic oscillations independent of the initial configuration. These modes are exponentially dampened, and can help us understand the dynamics and stability of BHs. Recently, we even got the first images capable of offering a visualization of these objects. BHs, due to their simplicity and extreme nature, possess enormous potential to answer other important questions in cosmology and other fields, as well as for the discovery of new physics.

In addition, there is a less well-known object inherently associated with the BH, namely the white hole (WH), which is the object possessing the past singularity in Fig. 1.1. Since Einstein's theory exhibits time-reversal symmetry, it must allow for an object with the reverse properties of a BH to be present in the maximal analytical solution. Born from this past singularity, this object expels everything inside it, and nothing from outside can cross the WH event horizon, located also at $r = 2M$ for the Schwarzschild metric.

Unfortunately, there are no known astrophysical phenomena or formation mechanisms analogous to gravitational collapse that can create these objects. There has never been a confirmed detection in our universe, despite the possibility of several candidates under appropriate conditions [10]. Unlike its close relative, WHs have not received much attention from the scientific community. These objects are indeed one of the most exotic and extreme ones ever proposed, raising many challenges in their physics, but so did BHs. With this in mind, the existence of WHs is still an open question, as well as their place in physics, and their role in the universe. Nevertheless, it is important to study WHs more thoroughly,

not only for their potential to address certain questions in cosmology, but also for their close connection with BHs. Indeed, some proposals have been made to connect these two objects in order to solve BHs physics challenges and create provoking possibilities [11, 12]. Some other works have been presented to solve some WH difficulties, where, for certain spacetimes, this object becomes a great candidate for the Big Bang. In addition to this provoking hypothesis, some authors have proposed that the formation of a BH leads to the creation of a WH/ Big Bang to originate a new universe [13, 14]. However, putting aside these proposals and looking at an isolated WH, there are still some important challenges for its existence: it typically possesses an erratic behaviour of continuous emission of matter, radiation and information, which has never been detected, and moreover raises difficult physical questions.

It is precisely the combination of these challenging aspects with great potential that motivates us to write this work. We will try to address both by making a detailed study of WHs in the case of the Schwarzschild metric. Amongst the different possibilities for time-reversed collapses originating WHs, there is a particular solution where this object recollapses into a black hole. This isolated time-reversed collapse/recollapse for the WH has been proposed in various contexts [15, 16, 17, 18], and brings us a step closer to understanding these objects.

The main purpose of this work is then to study WHs in Scharzschild under different initial conditions. We start by revising the maximal analytical solution for the WH for the simplest case possible, using the Schwarzschild metric. This study is useful for the later part of the work, especially for the construction of the Carter-Penrose diagrams. In addition, we also calculate the surface gravity for the WH.

Our next goal is to adapt the Oppenheimer-Snyder collapse, by matching a Friedman-Lemaître-Robertson-Walker (FLRW) universe with a WH, so that the Big Bang singularity shares the WH one. To do that, we start by thoroughly studying the FLRW metric, in the most general case including the cosmological constant, obtaining its Ricci tensor to write the Einstein field equations. Through the conservation of the stress-energy tensor, we proceed to deduce the Friedman equations and, consequently, study the possible behaviours of a spherical dust cloud described by this metric. The following step is to match this metric with the Schwarzschild-de Sitter solution (to consider the more general case). This allows us to match the reversed dust collapse with the WH so that one can ensure that these two together form a full solution of the Einstein field equations.

By solving the Friedman equations, we obtain three different behaviours of the surface of the dust cloud exiting the WH. We proceeded to study the reversed collapse case in more depth and its matching with the WH metric. We focus on the specific case where there is a recollapse leading to a BH, allowing the WH to have a finite lifetime, and solving one of their major problems. According to the different behaviours of the surface of the dust cloud, it is possible to obtain the Carter-Penrose diagrams for each case, thus improving the understanding of the matched solution. Again, we concentrate on the reverse collapse, considering different diagrams with or without the intersection of the WH and BH horizons.

In the following section, we focus on studying the dynamics of the WH by looking at scalar field and gravitational perturbations, whose equation of motion we obtain for the first case. This study primarily aims to find the quasinormal modes of the WH by adapting the boundary condition at the horizon for this object. We take the opportunity to analyse simpler potentials like Poschl-Tellller and Dirac delta, in preparation for considering the actual potential given by the Schwarzschild metric. In addition, we also consider approximated methods such as WKB, and conclude by trying to find the QNMs numerically using direct integration, a similar method to the one used by Chandrasekhar and Detweiler. Throughout this section, a parallel is always made for the BH. For both potentials, Poschl-Teller and Dirac delta, we were unable to find any QNMs. It was also not possible to find them using the WKB approximation or the direct integration method, indicating that, if these QNMs exist, they are very unusual and hard to find when comparing with the BH QNMs. After a thorough review of the literature, we found that a WH mode, defined here by the change in the horizon's boundary condition, has been considered. These modes have mostly been studied for the Kerr spacetime, as well as for its Schwarzschild limit, where they take a different form and can be obtained analytically. We have made a proposal to reinterpret these modes as being WH QNMs, providing physical arguments as well as support from independent work in this research area.

Throughout this work we will use geometrized units, that is, we will set $G = c = 1$.

2

Maximal analytical extension of a Schwarzschild white hole

In order to study the maximal analytical extension of the WH, we must revise Carter-Penrose diagrams [19]. To introduce this topic, which will be used throughout this thesis, one can start by defining the Minkowski metric in spherical coordinates, given by

$$ds^2 = -dt^2 + dr^2 + r^2 d\Omega^2, \tag{2.1}$$

where $d\Omega^2$ is the standard metric for S^2. After performing the change of coordinates for the retarded and advanced time parameters, respectively

$$\begin{aligned} u &= t - r, \\ v &= t + r, \end{aligned} \tag{2.2}$$

the metric presents the required form

$$ds^2 = -dudv + r^2 d\Omega^2. \tag{2.3}$$

These are null coordinates, and from $r = \frac{1}{2}(v - u)$ we see that $v \leq u$ since $r \geq 0$. Finally, to compactify the spacetime we use the change of coordinates given by

$$\begin{aligned} u &= \operatorname{arctanh}(\tilde{u}), \\ v &= \operatorname{arctanh}(\tilde{v}). \end{aligned} \tag{2.4}$$

This allows us to construct the Carter-Penrose diagram of the Minkowski spacetime [20]. To obtain the maximal analytical extension for the WH in the simplest possible way, one can start with the Schwarzschild metric given by

$$ds^2 = -f dt^2 + f^{-1} dr^2 + r^2 d\Omega^2, \quad \text{with} \quad f = 1 - \frac{2M}{r}, \tag{2.5}$$

where M is the mass of the BH. The following step is to perform a change of coordinates in the metric, putting it in the conformal form, and then choosing the WH region. This leads us to defining the Eddington-Finkelstein coordinates, as well as the retarded and advanced time parameters:

$$\begin{aligned} u &= t - \int \left(1 - \frac{2M}{r}\right)^{-1} dr = t - r - 2M \log|r - 2M|, \\ v &= t + \int \left(1 - \frac{2M}{r}\right)^{-1} dr = t + r + 2M \log|r - 2M|. \end{aligned} \tag{2.6}$$

Then to study the domain $r < 2M$ for the WH, one can write the metric as

$$ds^2 = \left(1 - \frac{2M}{r}\right) dudv = -\left(\frac{2M}{r} - 1\right) dudv', \tag{2.7}$$

where $v' = -v$, which leads to the coefficient being negative, as we desired for the conformal form. Therefore, we obtain

$$u + v' = -2r - 4M \log|r - 2M| \in (-4M \log(2M), +\infty), \tag{2.8}$$

and by setting

$$v'' = v' + 4M \log(2M), \tag{2.9}$$

we obtain

$$u + v'' > 0. \tag{2.10}$$

For the domain of $r > 2M$ the metric in (2.7) is already in the required form and we see that

$$v - u = 2r + 4M \log|r - 2M| \in (-\infty, +\infty). \tag{2.11}$$

Finally, using the coordinate transformation in (2.4) for both regions, the following diagrams can be obtained

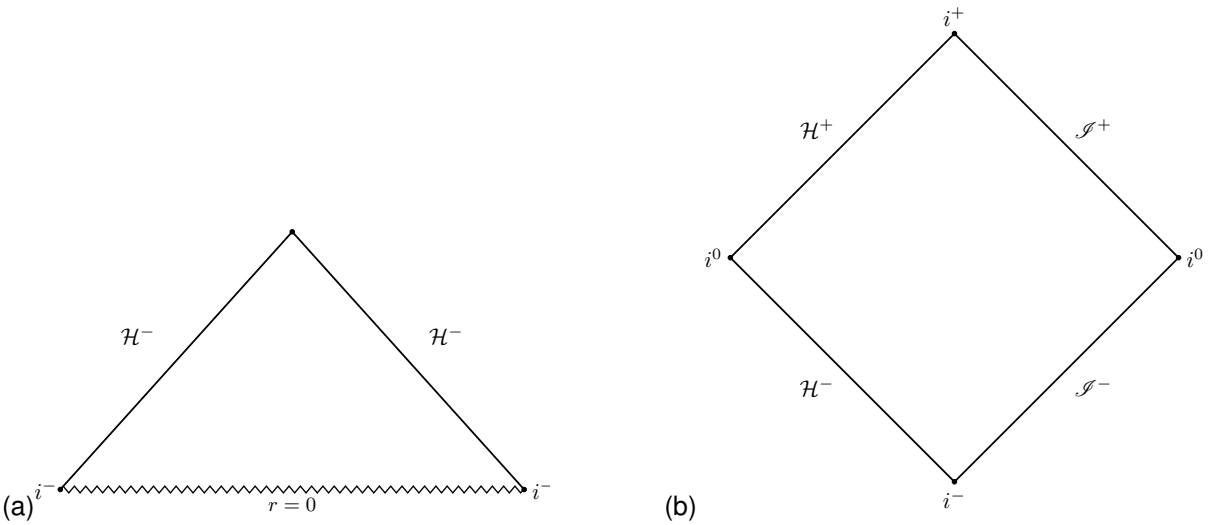

Figure 2.1: Carter-Penrose diagrams for (a): Schwarzschild WH region for $r < 2M$ possessing the past singularity, and for (b): the Schwarzschild exterior region for $r > 2M$.

Since we are only interested in the WH region, we can glue these two diagrams together by the past horizon, obtaining the result for the maximal analytical extension

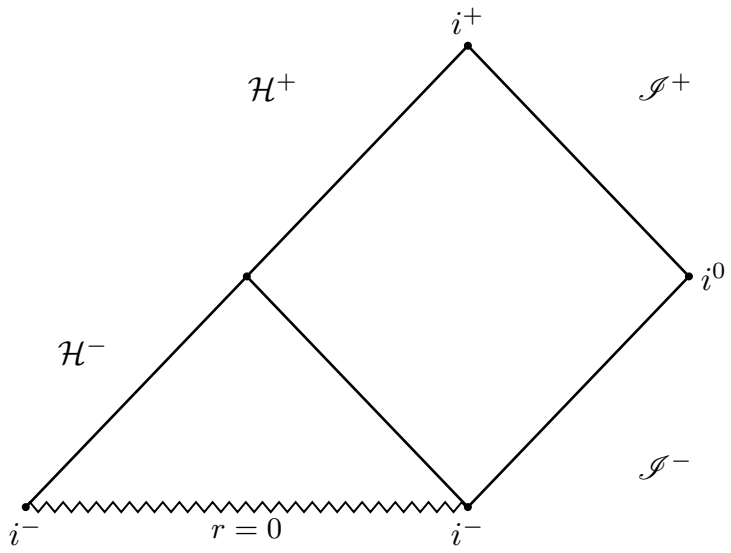

Figure 2.2: Carter-Penrose diagram for the maximal analytical extension of a Schwarzschild WH.

We can also obtain the maximal analytical solution for Schwarzschild, as it will be useful for the next section. By the same method we can take the region for $r < 2M$ and write the metric as

$$ds^2 = \left(1 - \frac{2M}{r}\right) dudv = -\left(\frac{2M}{r} - 1\right) du'dv, \tag{2.12}$$

with $u' = -u$. Analogously to what we did before for the WH we have,

$$u' + v = 2r + 4M \log|r - 2M| \in (-\infty, 4M \log(2M)), \tag{2.13}$$

which by setting

$$u'' = u' - 4M \log(2M) \tag{2.14}$$

we have

$$u'' + v < 0 \tag{2.15}$$

If we apply the coordinate rescaling (2.4), we obtain the triangle in Figure 2.3(a). This can be glued to the exterior region of $r > 2M$ to obtain the diagram for the domain of (v, r) represented in Figure 2.3(b)

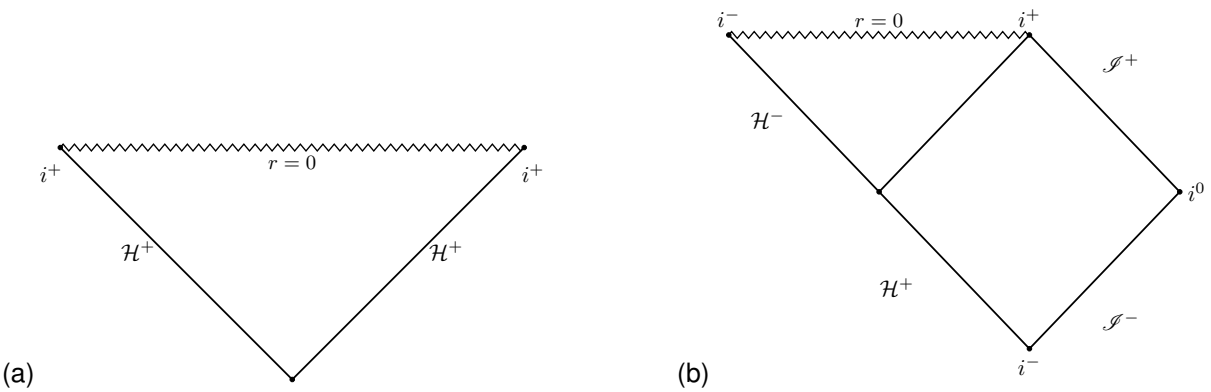

Figure 2.3: Carter-Penrose diagrams for (a): black hole region for $r < 2M$ possesing now the future singularity, and for (b): the glued diagram of the black hole with the exterior region.

We can also simultaneously glue both the black and WH regions for $r < 2M$ to the exterior region of $r > 2M$. In addition, since they are invariant under reflections with respect to $t = 0$, we can glue a mirror-reversed asymptotically flat region for $r > 2M$. This region glued to the last horizons $\mathcal{H}^+, \mathcal{H}^-$ represents a universe causally disconnected from the original region for $r > 2M$ and is united to this last one through a wormhole. This final diagram in Figure 2.4 represents the maximal analytical extension of Schwarzschild

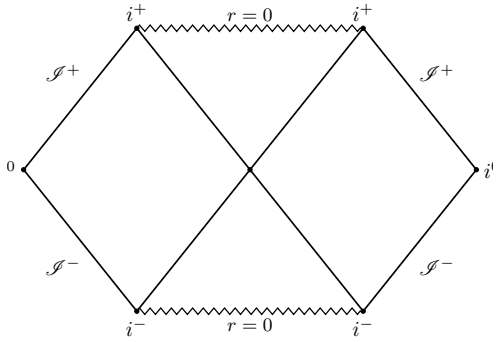

Figure 2.4: Carter-Penrose diagram for the maximal analytical extension of Schwarzschild spacetime.

Additionally, one can easily calculate the surface gravity for a WH, by first considering the Schwarzschild metric written in the retarded Eddington-Finkelstein coordinates (2.6), which takes the following form:

$$ds^2 = -f du^2 - 2du dr + r^2 d\Omega^2 \,. \tag{2.16}$$

The surface gravity at a Killing horizon is defined by

$$\eta^a \nabla_a \eta^b = k\eta^b \,, \tag{2.17}$$

where η^a is a suitably normalized Killing vector field. For the Schwarzschild in Schwarzschild coordinates we have $\eta^a = (1, 0, 0, 0)$, and when applying the change of coordinates mentioned above the Killing vector retains its form. Using Eq. (2.17), we arrive at

$$k = -\frac{1}{2}\frac{\partial}{\partial_r}\left(1 - \frac{2M}{r}\right). \tag{2.18}$$

Therefore, for the Schwarzschild WH with mass M, the surface gravity is $k = -\frac{1}{4M}$ as one could expect.

3

Time-reversed Oppenheimer-Snyder collapse for a white hole

3.1 Introduction

By following [21], one can understand the concepts necessary for the adaptations needed to turn the solution described in Fig. 3.1 into a WH.

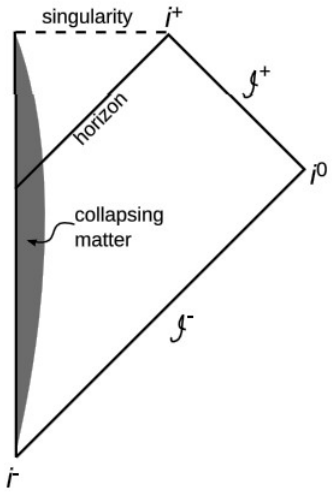

Figure 3.1: Carter-Penrose diagram for the Oppenheimer-Snyder collapse, representing a homogeneous and isotropic sphere of dust collapsing and forming a black hole, merging into Schwarzschild spacetime.

The objective here would be to time-reverse this solution in order for it to describe a WH. The dust sphere would come out of the singularity, from its collapsed state, and be expelled with radial symmetry through the event horizon. This otherwise can be seen as a sphere of dust coming out of an object possessing a singularity, the WH.

Looking at the diagram in Fig. 3.1, to obtain the behaviour described, one has to time reverse this collapse, which, by the nature of Einstein field equations, is still a solution. To reach this point, further analysis is necessary to obtain the behaviour of the dust sphere and the glueing with the WH solution to construct the Carter-Penrose diagram in detail. Here we will mainly follow [21, 19]

Firstly, the most important concept was to define the metrics, with one being the classic Schwarzschild metric. As for the one describing the interior of the dust sphere, the FLWR metric can be used in order to describe a homogeneous isotropic spacetime with spherical symmetry. These metrics are given by

$$ds_-^2 = -d\tau^2 + a^2(\tau)\left(\frac{1}{1-kr^2}dr^2 + r^2 d\Omega^2\right), \tag{3.1}$$

$$ds_+^2 = -f dt^2 + f^{-1}dr^2 + r^2 d\Omega^2, \quad \text{with} \quad f = 1 - \frac{2M}{r}. \tag{3.2}$$

Here, $a(\tau)$ represents the scale factor, k the curvature of the spatial sections, and t and τ both represent time, with different notation to avoid confusion.

3.2 The FLRW model

As one can see in the metric (3.1), k has not been fixed, and can have values of -1, 0 or 1 depending on the spatial geometry chosen. In addition, the scale factor $a(\tau)$ describes the temporal radial evolution of the dust sphere. To have a better understanding of this universe, one has to obtain the Friedman equations by solving the Einstein field equations, given by

$$R_{\mu\nu} - \frac{1}{2}g_{\mu\nu}R + \Lambda g_{\mu\nu} = 8\pi T_{\mu\nu}. \tag{3.3}$$

We consider the cosmological constant Λ to be nonzero for now. To obtain the Ricci tensor and scalar, we must first calculate the Christoffel symbols using (A.2). Taking into account the metric (3.1), defining $\partial_\tau a(\tau) = \dot{a}$ and writing $\tilde{g}_{ij}$ for the spatial metric divided by a^2, with $i, j = 1, 2, 3$, the non-zero Christoffel symbols are the following:

$$\begin{aligned}
&\Gamma^t_{ij} = \dot{a}a\tilde{g}_{ij} \quad ; \quad \Gamma^i_{tj} = \frac{\dot{a}}{a}\delta^i_j; \\
&\Gamma^r_{rr} = \frac{kr}{1-kr^2} \quad ; \quad \Gamma^r_{\theta\theta} = -r(1-kr^2) \quad ; \quad \Gamma^r_{\phi\phi} = -r\sin^2\theta(1-kr^2); \\
&\Gamma^\theta_{r\theta} = \Gamma^\theta_{\theta r} = \Gamma^\phi_{r\phi} = \Gamma^\phi_{\phi r} = \frac{1}{r}; \\
&\Gamma^\theta_{\phi\phi} = -\sin\theta\cos\theta \quad ; \quad \Gamma^\phi_{\phi\theta} = \Gamma^\phi_{\theta\phi} = \frac{1}{\tan\theta}.
\end{aligned} \tag{3.4}$$

Given all the Christoffel symbols, one can obtain the Ricci tensor to reach the Einstein equations. The only nonzero Ricci tensor components, given by (A.1), are

$$R_{tt} = -3\frac{\ddot{a}}{a}; \tag{3.5}$$

$$R_{rr} = \frac{a\ddot{a}}{1-kr^2} + \frac{2\dot{a}^2}{1-kr^2} + \frac{2k}{1-kr^2} = \frac{g_{rr}}{a^2}(\ddot{a}a + 2\dot{a}^2 + 2k); \tag{3.6}$$

$$R_{\theta\theta} = \frac{g_{rr}}{a^2}(\ddot{a}ar^2 + 2\dot{a} + 2k); \tag{3.7}$$

$$R_{\phi\phi} = \ddot{a}ar^2\sin^2\theta + 2\dot{a}^2r^2\sin^2\theta + 2kr^2\sin^2\theta = \frac{g_{\phi\phi}}{a^2}(\ddot{a}ar^2 + 2\dot{a} + 2k). \tag{3.8}$$

From these components, we find that the Ricci scalar is given by

$$R = g^{\mu\nu}R_{\mu\nu} = \frac{6}{a^2}(\ddot{a}a + \dot{a}^2 + k). \tag{3.9}$$

Before writing the equations, one has to define the energy-momentum tensor $T_{\mu\nu}$ for our case, which is a homogeneous and isotropic sphere of pressureless dust, having four-velocity $u_\mu = (1, 0, 0, 0)$, which

leads to the only nonvanishing component being

$$T_{tt} = \rho(\tau), \tag{3.10}$$

with $\rho(\tau)$ being the density of the sphere. Therefore, the temporal part of the equation (3.3) gives

$$-3\frac{\ddot{a}}{a} + 3\frac{\ddot{a}}{a} + 3\left(\frac{\dot{a}}{a}\right)^2 + 3\frac{k}{a^2} - \Lambda = 8\pi\rho(\tau), \tag{3.11}$$

which can be transformed into

$$\left(\frac{\dot{a}}{a}\right)^2 = \frac{8\pi\rho(\tau) + \Lambda}{3} - \frac{k}{a^2}. \tag{3.12}$$

For the spatial part, using Eq. (3.12) we obtain

$$\frac{\ddot{a}}{a} = \frac{\Lambda - 4\pi\rho(\tau)}{3}. \tag{3.13}$$

Another important law, which is very useful for our work, is the conservation of the stress-energy tensor, given by

$$T^{\mu\nu}_{;\nu} = T^{\mu\nu}_{,\nu} + \Gamma^{\mu}_{\nu\alpha}T^{\alpha\nu} + \Gamma^{\nu}_{\nu\alpha}T^{\mu\alpha} = 0. \tag{3.14}$$

By looking at the case of $\mu = \tau$ and taking into account (3.10) one gets

$$\partial_\tau\rho(\tau) + 3\frac{\rho(\tau)}{a(\tau)}\partial_\tau a(\tau) = 0, \tag{3.15}$$

which after some algebra gives us

$$\rho(\tau)a^3(\tau) = \beta, \tag{3.16}$$

with β being a constant. Finally, we can use this result in Eq. (3.12) and solve with respect to $\dot{a}$ to get

$$\dot{a}^2 = \frac{8\pi\beta}{3a} + \frac{a^2\Lambda}{3} - k. \tag{3.17}$$

This equation is fairly complex, and it would be very difficult to obtain an analytical solution. However, to have a better understanding of $a(\tau)$ one can see this equation above as the conservation of energy of a particle moving in a one-dimensional effective potential defined as

$$V(a) = -\left(\frac{8\pi\beta}{3a} + \frac{a^2\Lambda}{3}\right), \tag{3.18}$$

with energy $-k$. To understand the behaviour of $a(\tau)$, one can plot the effective potential $V(a)$ for 3 different values of $\frac{8\pi\beta}{3} = A$ after setting $\Lambda = 3$ (which corresponds to taking the cosmological radius as the length unit), and then plot the constant energy lines for each value of $k = -1, 0, 1$:

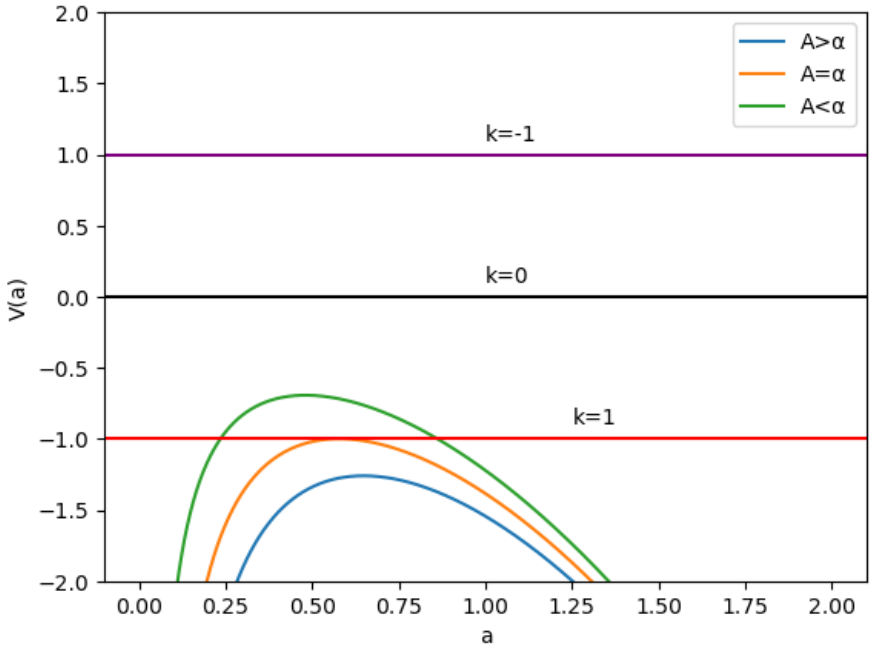

Figure 3.2: Effective potential for the Friedman equation, having 3 horizontal lines representing the kinetic energy for the three different values of k possible. In addition, we represent the potential for three different initial conditions around the red horizontal line of $k = 1$. These three representations indicate all the possible behaviours that this universe can have: a spherical or de Sitter-like universe (green), an Einstein universe (orange), and a hyperbolic or flat universe (blue).

One can easily see that there is a critical value for the case where $k = 1$, given by $\alpha = \frac{\sqrt{3}}{9}$. It is possible to see that for the blue case, we have similar behaviour to the hyperbolic and flat universes where $a(\tau)$ increases over time. For the orange case, we have an unstable equilibrium, where the attraction force is matched by the repulsion force of the cosmological constant, giving rise to the Einstein universe. Finally, the green curve shows us that, depending on the initial conditions, we can have a de Sitter-like universe or, our main focus due to the reasons mentioned in the introduction, the spherical model, where the sphere of dust reaches a maximum radius and recollapses to a singularity.

3.3 Matching

3.3.1 Extrinsic curvature

We now show how to obtain a single solution by matching the Schwarzschild and FLRW metrics along a surface that we will call S. To do this, we have to check that their extrinsic curvature is equal on both sides of the surface S. We can use one of the definitions of the second fundamental form as a Lie derivative, given by

$$K = \frac{1}{2}\mathcal{L}_n g_{|TS}\,. \tag{3.19}$$

From here on, we mainly follow [20], evaluating the Lie derivative at a certain hypersurface in the FLRW side, which we shall call S_1. In this case, we choose S_1 by fixing $r \equiv \sigma = \sigma_0$ (we change the name of the radial coordinate to avoid confusion with the radial coordinate in Schwarzschild), and write the induced FLRW metric as

$$ds^2_{|_{S_1}} = -d\tau^2 + a^2(\tau)\left(\sigma_0^2 d\theta^2 + \sigma_0^2 \sin^2\theta d\phi^2\right). \tag{3.20}$$

As a consequence, we have the following normal vector to the surface S_1:

$$n = \frac{\sqrt{1-k\sigma^2}}{a(\tau)}\frac{\partial}{\partial\sigma}. \tag{3.21}$$

Using Cartan's magic formula, one can compute the Lie derivative, given as

$$\mathcal{L}_X\omega = i_X d\omega + d(i_X\omega). \tag{3.22}$$

The Lie derivative for the $d\tau$ and dr components of the metric is zero in both cases, since we are evaluating the derivative at S_1. Therefore, the non zero components are given by $d\theta$ and $d\phi$

$$\mathcal{L}_n(a^2(\tau)\sigma^2 d\theta^2) = 2a(\tau)\sigma\sqrt{1-k\sigma^2}d\theta^2, \tag{3.23}$$

$$\mathcal{L}_n(a^2(\tau)\sigma^2\sin^2\theta d\phi^2) = 2a(\tau)\sigma\sqrt{1-k\sigma^2}\sin^2\theta d\phi^2. \tag{3.24}$$

Finally, when summing all the components we get

$$K_- = a(\tau)\sigma_0\sqrt{1-k\sigma_0^2}(d\theta^2 + \sin^2\theta d\phi^2). \tag{3.25}$$

Moving on to the other metric, we use the more general Schwarzschild-de Sitter metric to possibly include a cosmological constant:

$$ds^2_+ = -H(r)dt^2 + H(r)^{-1}dr^2 + r^2 d\Omega^2, \quad \text{with} \quad H(r) = 1 - \frac{2M}{r} - \frac{\Lambda r^2}{3}. \tag{3.26}$$

Similar to what we did before, we choose a spherically symmetric timelike hypersurface, S_2 using a parametrization of the form

$$\begin{cases} t = t(\tau) \\ r = r(\tau) \end{cases} \tag{3.27}$$

(their exact form of these functions is left to the matching conditions). We have a first constrain coming from the timelike property, and assuming the parametrization to be by proper time:

$$-H\dot{t}^2 + H^{-1}\dot{r}^2 = -1. \tag{3.28}$$

Using this condition, we can then write our induced metric as

$$ds_+^2 = -d\tau^2 + r^2(\tau)(d\theta^2 + \sin^2\theta d\phi^2). \tag{3.29}$$

When comparing with the metric in (3.20) we obtain the first matching condition:

$$r(\tau) = a(\tau)\sigma_0. \tag{3.30}$$

Since S_1 is ruled by timelike geodesics, so does S_2, and so in addition $r(\tau)$ and $t(\tau)$ must also satisfy the radial geodesic equation. Therefore, using (3.28) and the Euler-Lagrange equations, we get

$$\begin{cases} H\dot{t} = E \\ -H\dot{t}^2 + H^{-1}\dot{r}^2 = -1 \end{cases} \Leftrightarrow \begin{cases} H\dot{t} = E \\ \dot{r}^2 = E^2 - 1 + \frac{2M}{r} + \frac{\Lambda r^2}{3} \end{cases} . \tag{3.31}$$

To assure that equations (3.30), (3.31) and the Friedman equation (3.17) are compatible, we must then have

$$\begin{cases} E = \sqrt{1 - k\sigma_0^2} \\ M = \sigma_0^3 \frac{4\pi\beta}{3} \end{cases} . \tag{3.32}$$

This requires that $1 - k\sigma_0^2 > 0$, and it is easily shown that the mass parameter in the Schwarzschild-de Sitter spacetime is related to the density by

$$M = \frac{4\pi}{3} r^3(\tau)\rho(\tau). \tag{3.33}$$

To calculate the extrinsic curvature, we can consider a family of spherical shells, including S_2, with s being the parameter indexing the shells. To take the following step one needs to employ the Gauss Lemmas stated in Appendix B, which lead to writing the metric as

$$ds_+^2 = -d\tau^2 + A^2(\tau, s)ds^2 + r^2(\tau, s)(d\theta^2 + \sin^2\theta d\phi^2)\,. \tag{3.34}$$

Notice that the normal vector now takes the form

$$n = \frac{1}{A}\frac{\partial}{\partial s}\,. \tag{3.35}$$

Using Cartan's magic formula (3.22), the second fundamental form becomes

$$\begin{aligned} K_+ &= \frac{1}{2}(i_n dg + d(i_n g))_{|TS_2} \\ &= r(n \cdot r)(d\theta^2 + \sin^2\theta d\phi^2)\,. \end{aligned} \tag{3.36}$$

On the other hand, we can also write n in Schwarzchild-de Sitter coordinates as

$$n = -H^{-1}\dot{r}\frac{\partial}{\partial t} + H\dot{t}\frac{\partial}{\partial r}\,, \tag{3.37}$$

in order for it to be unit and orthogonal to

$$\dot{t}\frac{\partial}{\partial t} + \dot{r}\frac{\partial}{\partial r}\,. \tag{3.38}$$

Therefore, using this form for n and taking into account equation (3.31) and (3.32) one obtains

$$K_+ = r(\tau)\sqrt{1 - k\sigma_0^2}(d\theta^2 + \sin^2\theta d\phi^2)\,, \tag{3.39}$$

which by the matching condition (3.30) shows that the extrinsic curvatures are equal for both metrics. Therefore, one has shown that one can glue these metrics to obtain a solution of the Einstein equations.

3.3.2 Carter-Penrose diagrams

In this section, we take $\Lambda = 0$ for simplicity. Our objective is to construct the Carter-Penrose diagram for the solution resulting from matching the metric (3.1) to the Schwarzschild metric (3.2). In the case of no recollapse, for instance, with $k = 0$, we can assume that all solutions are defined for $\tau > 0$, with a true singularity at $\tau = 0$ (the Big Bang). Then one can write the metric (3.1) as

$$\begin{aligned} ds_-^2 &= -d\tau^2 + a^2(\tau)[d\rho^2 + \rho^2 d\Omega^2] \\ &= a^2(\tau)[-dt^2 + d\rho^2 + \rho^2 d\Omega^2] \\ &= a^2(\tau)[-dt^2 + d\rho^2] + r^2 d\Omega^2\,, \end{aligned} \tag{3.40}$$

with $\rho \in [0, +\infty)$ and $r = a(\tau)\rho$. Setting $\frac{8\pi\beta}{3} = A$, we have

$$\int_0^{+\infty} \frac{d\tau}{a(\tau)} = \int_0^{+\infty} \frac{da}{a\dot{a}} = \int_0^{+\infty} \frac{da}{a\sqrt{\frac{A}{a}}} = +\infty\,. \tag{3.41}$$

Therefore, the metric is conformal to the region $(0, +\infty) \times [0, +\infty)$ of the Minkowski spacetime. With this information from the FLRW diagram, one can match it with the Schwarzschild diagram shown in Fig. 2.2 to obtain the Carter-Penrose diagram depicted in the following figure.

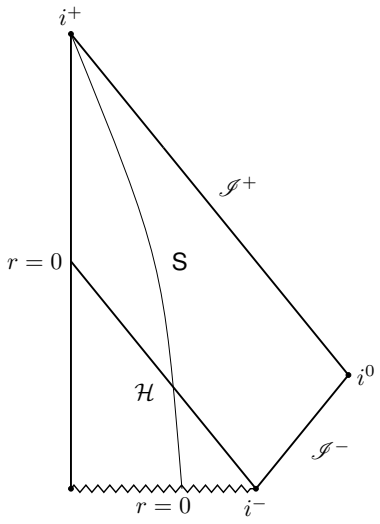

Figure 3.3: Carter-Penrose diagram for the FLRW universe matched to the Schwarzschild WH region. The diagram represents a homogenous, isotropic sphere of dust expanding radially out of the WH, from its collapsed state and continuing to do so through infinity.

We now move on to the spherical universe, the case with recollapse that we want to focus on. As we have seen in Fig. 3.2, one has to consider $k = 1$, and so that we can rewrite (3.1) as

$$\begin{aligned} ds_-^2 &= -d\tau^2 + a^2(\tau)[d\psi^2 + \sin^2\psi\, d\Omega^2] \\ &= a^2(\tau)[-dt^2 + d\psi^2 + \sin^2\psi\, d\Omega^2] \\ &= a^2(\tau)[-dt^2 + d\psi^2] + r^2 d\Omega^2\,, \end{aligned} \tag{3.42}$$

where $\psi \in [0, \pi]$, $r = a(\tau)\sin\psi$ and

$$t = \int_0^\tau \frac{d\tau}{a(\tau)}. \tag{3.43}$$

Since we are in the recollapsing case, there exists a t_{max} such that, using Eq. (3.17), one obtains

$$t = \int_0^{\tau_{\max}} \frac{d\tau}{a(\tau)} = 2\int_0^{a_{\max}} \frac{da}{a\dot{a}} = 2\int_0^A \frac{da}{a\sqrt{\frac{A}{a}-1}} = 2\pi\,. \tag{3.44}$$

Therefore, the metric is conformal to the region $(0, 2\pi) \times [0, \pi]$ of the Minkowski spacetime. This case is fairly more complex, and deserves more attention since we matched this metric with the Schwarzschild metric. One of the aspects to be careful about is determining where or if the horizons meet in the final Carter-Penrose diagram. To do that, one can start by noticing that these horizons are ruled by radial null geodesics in FLRW, leading to

$$\int_{\sigma_i}^{\sigma_0} \frac{d\sigma}{\sqrt{1-\sigma^2}} = \int_{\tau_i}^{\tau_0} \frac{d\tau}{a(\tau)} = \int_{a_i}^{a_0} \frac{da}{a\dot{a}} = \int_{a_0}^{a_i} \frac{da}{a\sqrt{\frac{A}{a}-1}}, \tag{3.45}$$

where these integrals are being evaluated from the intersection of the horizons to the surface S where we have the condition (3.30), leading to $a_0 = 2M/\sigma_0$. For a_i this must be the maximum of the function, where the sphere starts to contract, which is given by A. Finally, by solving the integrals and using (3.32) one obtains

$$\arcsin(\sigma_0) - \arcsin(\sigma_i) = 2\arctan\left(\sqrt{\frac{1}{\sigma_0^2} - 1}\right). \tag{3.46}$$

Therefore the condition for the horizons to intersect is

$$\arcsin(\sigma_0) > 2\arctan\left(\sqrt{\frac{1}{\sigma_0^2} - 1}\right). \tag{3.47}$$

This condition may or may not be satisfied, depending on the initial conditions chosen, and so it is possible to construct the two following variants of the Carter-Penrose diagrams:

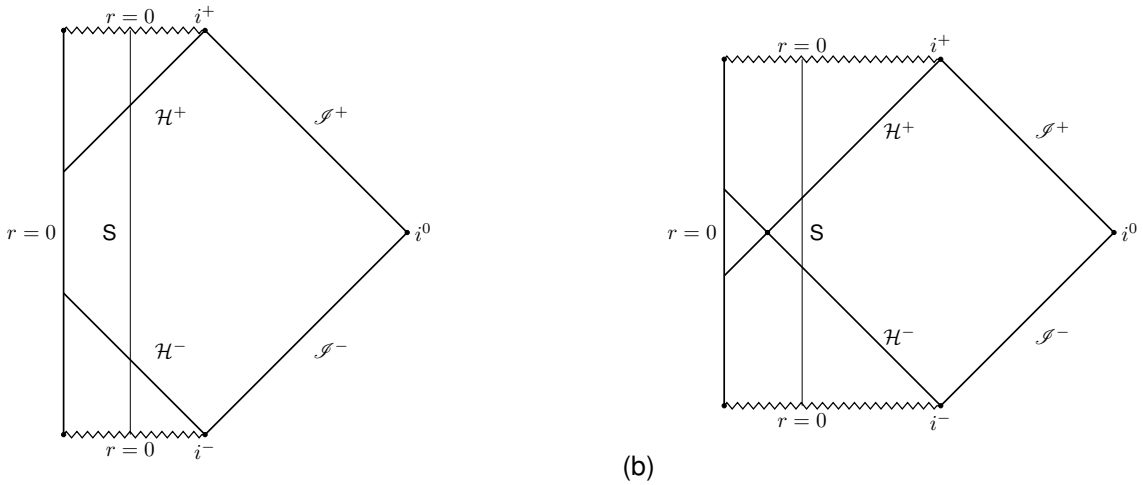

Figure 3.4: Carter-Penrose diagrams for (a): FLRW recollapsing universe matched to a Schwarzschild exterior in the case where the horizons do not intersect and (b): FLRW recollapsing universe matched to a Schwarzschild exterior with the intersection of the horizons inside the FLRW region. For both diagrams, we have a homogeneous, isotropic sphere of dust expanding radially through the event horizon, but eventually slowing down, reaching a maximum radius, and then collapsing to create a black hole.

Having obtained all the diagrams, one can have a complete understanding of all possible solutions, their outcomes, and evolutions. Now, one can try and study the details and obtain more information about them, starting from studying the dynamics and stability.

4

White hole QNMs: toy models

4.1 The wave equation

In the next sections, we will study the dynamics of the WH. To do that, we will start by trying to find the quasinormal modes analytically using toy models. We will focus primarily on scalar and gravitational perturbations, and we will look for QNMs of a WH, which is essential for us to understand the dynamics of this object. To obtain these results, we propose a change in the boundary condition at the horizon, and interpret the results as being the ones from a WH.

We start this segment by considering a simplified action from [22] involving a complex scalar field with mass $m_S = \mu\hbar$:

$$S = \int d^4x\sqrt{-g}\left(\frac{1}{2k}(R-2\Lambda) - \frac{1}{2}g^{\mu\nu}\Psi^*_{,\mu}\Psi_{,\nu} - \frac{\mu^2}{2}\Psi^*\Psi\right). \tag{4.1}$$

We can then separate the Lagrangian into two terms, the scalar field Lagrangian and the Einstein-Hilbert Lagrangian $\frac{R}{2k} - \frac{\Lambda}{k}$. By varying this action with respect to Ψ, one can easily obtain the Klein-Gordon equation:

$$(\Box - \mu^2)\Psi = 0\,. \tag{4.2}$$

In order to separate Eq. (4.2) one can use the ansatz in [23] to write Ψ as

$$\Psi(t,r,\theta,\phi) = \sum_{l,m}\int d\omega e^{-i\omega t}\frac{R(r)}{r}Y_{lm}(\theta,\phi)\,, \tag{4.3}$$

where $Y_{lm}(\theta,\phi)$ are the spherical harmonics. The next step is to consider the metric (3.2) and use the tortoise coordinate r^* defined by $dr/dr^* = f(r)$ to obtain the equation

$$\left[\frac{d^2}{d^2r^*} + \left(\omega^2 - V(r)\right)\right]R(r) = 0\,, \tag{4.4}$$

with

$$V(r) = f(r)\left(\mu^2 + \frac{l(l+1)}{r^2} + \frac{f'(r)}{r}\right) \tag{4.5}$$

and

$$\left(\partial_\theta^2 + \cot\theta\partial_\theta\right)Y_{lm}(\theta) + \left(l(l+1) - \frac{m^2}{\sin^2\theta}\right)Y_{lm}(\theta) = 0\,. \tag{4.6}$$

The general form of Eq. (4.5) defined in [24] shows not only the dimension and Λ dependency of this equation, but, most importantly, the spin of the type of perturbation. The most important values for the spin are $s = 0, \pm1, \pm2$, representing scalar, electromagnetic, and gravitational perturbations, respectively. That way, in a 4-dimensional spacetime, the most general way to represent the potential is given by

$$V(r) = f(r)\left(\frac{l(l+1)}{r^2} + (1-s^2)\left(\frac{f'(r)}{r} - \frac{(4-s^2)\Lambda}{2}\right)\right). \tag{4.7}$$

As one can see, the full form of Eq. (4.4) with the Regge-Wheeler potential (4.5) is fairly complex and difficult to study. To prepare the following sections, we will consider different and increasingly more complex potentials for equation (4.4) to study the existence of quasinormal modes. In regards to the boundary conditions, we will adapt them in order to emulate a WH by always imposing outgoing behaviour at the analogue of the event horizon.

4.2 Delta-function potential

Let us consider the general form of Eq. (4.4) having $\mu = 0$, with the potential now given by a Dirac delta, leading to the following equation:

$$\frac{\partial^2\psi}{\partial r_*^2} - \frac{\partial^2\psi}{\partial t^2} - V_0\delta(r_*)\psi = 0. \tag{4.8}$$

To begin solving this equation, one can start by using the Laplace transform, defined as

$$\mathcal{L}f(s) = \int_0^{+\infty} e^{-st} f(t)dt\,, \tag{4.9}$$

where we can consider s to have the form $-i\omega$. By applying the Laplace transform to Eq. (4.8) one obtains

$$\frac{d^2\tilde{\Psi}}{dr_*^2} + \left(\omega^2 - V_0\delta(r_*)\right)\tilde{\Psi} = i\omega\psi(t=0) = I(r_*)\,. \tag{4.10}$$

Here we have considered the scalar field to be initially static, so that $\partial_t\psi(t=0) = 0$. The next step is to define two independent solutions, for two separate regions of the potential, given by

$$\widetilde{\Psi}_L = \begin{cases} e^{i\omega r_*} \quad , & r_* \to -\infty \\ Ae^{-i\omega r_*} + Be^{i\omega r_*}, & r_* \to \infty \end{cases} . \tag{4.11}$$

$$\widetilde{\Psi}_R = e^{i\omega r_*} \quad , \quad r_* \to \infty \tag{4.12}$$

Since we are considering a WH, we have reversed the BH boundary conditions ($e^{-i\omega r_*}$) by imposing only outgoing waves at the horizon. In addition, to impose continuity at $r_* = 0$, we can infer that $1 = A + B$. From here one can integrate Eq. (4.10) in the interval $(-\epsilon, \epsilon)$, which by taking the limit when $\epsilon \to 0$ yields

$$\partial_{r_*}\widetilde{\Psi}|_{-\epsilon}^{+\epsilon} = V_0\widetilde{\Psi}(r_* = 0)\,. \tag{4.13}$$

Which leads to the following equation:

$$\partial_{r_*}\widetilde{\Psi}_{L_+}(0) - \partial_{r_*}\widetilde{\Psi}_{L_-}(0) = V_0\widetilde{\Psi}(r_* = 0)\,. \tag{4.14}$$

With $\widetilde{\Psi}(r_* = 0) = 1$ and assuring continuity along the two solutions in (4.11), one arrives at the following system of equations:

$$\begin{cases} 1 = A + B \\ B - A - 1 = \frac{V_0}{i\omega} \end{cases} \Leftrightarrow \begin{cases} B = 1 - \frac{iV_0}{2\omega} \\ A = \frac{iV_0}{2\omega} \end{cases} . \tag{4.15}$$

After explicitly obtaining A and B, one can start to look at the approximate solution for a distant observer. For simplicity, we consider the solution of $\widetilde{\Psi}$ for large distances, given by

$$\widetilde{\Psi}_{r_* \to \infty} = \widetilde{\Psi}_R \int_{-\infty}^{+\infty} \frac{I(r_*)}{W} \widetilde{\Psi}_L dr_* \,, \tag{4.16}$$

where

$$W_{\text{WH}} = 2\omega i A = 2\omega i \left(\frac{iV_0}{2\omega} \right) = -V_0 \,. \tag{4.17}$$

This result implies that there are no poles in the integral for these boundary conditions. Therefore, it is not possible to obtain the quasinormal modes for this type of potential. This result already shows a major difference when compared to the BH case where we have

$$W_{\text{BH}} = 2\omega i A_{\text{BH}} = 2\omega i - V_0 \,, \tag{4.18}$$

indicating that there is a QNM for $\omega = -iV_0/2$. Nonetheless, one can still try to consider a faraway observer and find the approximated solution for large distances:

$$\widetilde{\Psi}_{r_* \to \infty} = \widetilde{\Psi}_R \int_{-\infty}^{+\infty} \frac{I(r_*)}{W} \widetilde{\Psi}_L dr_* = \frac{e^{i\omega r_*}}{2A} \int_{-\infty}^{+\infty} \psi(t=0) \left(A e^{-i\omega r_*} + B e^{i\omega r_*} \right) dr_* \,. \tag{4.19}$$

Here we consider a solution with initial data $\psi(t = 0) = \delta(r_* - r_0)$ to solve the integral, obtaining

$$\widetilde{\Psi}_{r_* \to \infty} = \frac{e^{i\omega(r_* - r_0)}}{2} + \frac{B}{2A} e^{i\omega(r_* + r_0)} \,. \tag{4.20}$$

By inverting the Laplace transform, we have

$$\psi_{r_* \to \infty} = \frac{1}{4\pi} \int_{-\infty}^{+\infty} e^{i\omega(r_* - r_0 - t)} d\omega + \frac{1}{4\pi} \int_{-\infty}^{+\infty} \frac{B}{A} e^{i\omega(r_* + r_0 - t)} d\omega \,. \tag{4.21}$$

Using the definition of the Dirac delta as an improper integral, the equation becomes

$$\psi_{r_* \to \infty} = \frac{1}{2} \delta(r_* - r_0 - t) - \frac{i}{4\pi V_0} \int_{-\infty}^{+\infty} (2\omega - iV_0) \, e^{i\omega(r_* + r_0 - t)} d\omega \,. \tag{4.22}$$

When looking at the integral, there is a necessary condition for it to be non-zero, given by $t > r_* + r_0$, due to the time shift presented in the exponential. For simplicity, we can define $a = a(r_*, t) = r_* + r_0 - t$

so that we can write

$$
\begin{aligned}
-\frac{i}{4\pi V_0}\int_{-\infty}^{+\infty}(2\omega - iV_0)\,e^{i\omega a}d\omega &= -\frac{1}{2}\int_{-\infty}^{+\infty}\frac{e^{i\omega a}}{2\pi}d\omega - \frac{i}{2\pi V_0}\int_{-\infty}^{+\infty}\omega e^{i\omega a}d\omega \\
&= -\frac{1}{2}\delta(r_* + r_0 - t) - \frac{i}{2\pi V_0}\int_{-\infty}^{+\infty}\omega e^{i\omega a}d\omega\,.
\end{aligned}
\tag{4.23}
$$

Here, again, we have used the definition of the Dirac delta and are left with the last integral. However, one can look at the integral in (4.23) as the inverse Fourier transform of the function $i\omega$. The inverse Fourier transform of this function is well established and results in

$$
-\frac{1}{V_0}\delta'(a) = -\frac{1}{V_0}\delta'(r_* + r_0 - t)\,. \tag{4.24}
$$

Therefore, the solution is finally given by

$$
\psi^{\text{WH}}_{r_*\to\infty} = \begin{cases} \frac{1}{2}\delta(r_* - r_0 - t) \quad , \quad t < r_* + r_0 \\ \\ \frac{1}{2}\delta(r_* - r_0 - t) - \frac{1}{2}\delta(r_* + r_0 - t) - \frac{1}{V_0}\delta'(r_* + r_0 - t), \quad t > r_* + r_0 \end{cases} . \tag{4.25}
$$

We can also compare this result with the BH case with $V = 2V_0\delta(r_*)$ having

$$
\psi^{\text{BH}}_{r_*\to\infty} = \begin{cases} \frac{1}{2}\delta(r_* - r_0 - t) \quad , \quad t < r_* + r_0 \\ \\ \frac{1}{2}\delta(r_* - r_0 - t) + \frac{V_0}{2}e^{V_0(r_* + r_0 - t)}, \quad t > r_* + r_0 \end{cases} . \tag{4.26}
$$

When comparing these two solutions, Eqs. (4.25) and (4.26), we see that both contain half of the initial signal moving towards the right. However, there is a clear distinction in the signal that initially travels in the other direction. For simplicity, let us consider $r_0 > 0$, so that half of our initial condition propagates towards infinity, representing our first term. The difference in behaviour occurs when the other half of the signal, traveling in the opposite direction, interacts with the potential. Due to the boundary condition for the BH, the resulting term is a negative exponential, where the signal dissipates over time, which agrees with the fact that there is a BH QNM. This is completely different for the WH solution, which has no QNMs. Due to the boundary condition on the WH horizon, the terms resulting from the interaction have non-decaying properties, representing a combination of signals propagating to infinity. However, the functions that represent these signals are non-smooth and difficult to interpret. To remedy this, we can consider a different initial condition for this potential. After obtaining equation (4.19) for the approximated solution, instead of using a Dirac delta for $\psi(t = 0)$, one can use a Gaussian function of the form $\gamma e^{-\alpha(r_* - r_0)^2}$. Using this initial condition, one can identify the integrals as the Fourier transform

of the Gaussian. In this case, Eq. (4.19) takes the form

$$\begin{aligned}
\widetilde{\Psi}_{r_*\to\infty} =& \frac{e^{i\omega r_*}}{2A}\int_{-\infty}^{+\infty}\gamma e^{-\alpha(r_*-r_0)^2}\left(Ae^{-i\omega r_*}+Be^{i\omega r_*}\right)dr_* \\
=& \frac{e^{i\omega r_*}}{2}\gamma\int_{-\infty}^{+\infty}e^{-\alpha(r_*-r_0)^2}e^{-i\omega r_*}dr_* + e^{i\omega r_*}\frac{B}{2A}\gamma\int_{-\infty}^{+\infty}e^{-\alpha(r_*-r_0)^2}e^{i\omega r_*}dr_* \\
=& \frac{e^{i\omega r_*}}{2}\gamma\int_{-\infty}^{+\infty}e^{-\alpha(r_*-r_0)^2}e^{-i\omega r_*}dr_* - e^{i\omega r_*}\frac{i\omega}{V_0}\gamma\int_{-\infty}^{+\infty}e^{-\alpha(r_*-r_0)^2}e^{i\omega r_*}dr_* \\
& -e^{i\omega r_*}\frac{1}{2}\gamma\int_{-\infty}^{+\infty}e^{-\alpha(r_*-r_0)^2}e^{i\omega r_*}dr_* \\
=& \left(\frac{1}{2}\left(e^{i\omega(r_*-r_0)}-e^{i\omega(r_*+r_0)}\right)-\frac{i\omega e^{i\omega(r_*+r_0)}}{V_0}\right)\sqrt{\frac{\pi}{\alpha}}\gamma e^{-\frac{\omega^2}{4\alpha}}\,.
\end{aligned} \tag{4.27}$$

Then one can invert the Laplace transform, leading to

$$\psi^{\mathsf{WH}}_{r_*\to\infty} = \begin{cases} \frac{1}{2}\gamma e^{-\alpha(r_*-r_0-t)^2} \quad , \quad t < r_*+r_0 \\ \frac{1}{2}\gamma e^{-\alpha(r_*-r_0-t)^2} - \frac{1}{2}\gamma e^{-\alpha(r_*+r_0-t)^2} + \frac{2\gamma\alpha}{V_0}(r_*+r_0-t)e^{-\alpha(r_*+r_0-t)^2}, \quad t > r_*+r_0 \end{cases} . \tag{4.28}$$

When comparing Eq.(4.28) to Eq. (4.25), we can see the clear similarities between them, where for each Dirac delta we now have a gaussian, showing us smooth terms for our approximate solution. We can now analyze and physically interpret the solution obtained for the WH. At the start, as we described earlier, the solution is trivial. It is when the incoming wave reaches the potential at $t = r_* + r_0$ that we can see the effects of the WH. Fig. (4.1) gives a clearer representation of the BH and WH cases. Due to our WH boundary condition, we are imposing outgoing waves coming out of the horizon at $r = 2M$. These signals moving towards the potential will also interact with the signal coming from our initial condition. The WH boundary condition is fairly strong, in the sense that these outgoing waves will prevent any ingoing signals from reaching the horizon by interacting with them. That is essentially what is happening in the second part of the solution in Eq. (4.28). At the Dirac delta potential, the incoming half gaussian is totally reflected from this interaction with the outgoing terms through the potential, and a second term also rises from this interaction. Looking at the last term, we see that the value of V_0 plays the role of a regulator of this signal. As $V_0 \to 0$ this term explodes, indicating that, without a potential, an infinitely strong signal would be needed to interact with our initial condition. Inversely, for large values of V_0 we would see this last term reaches very small values.

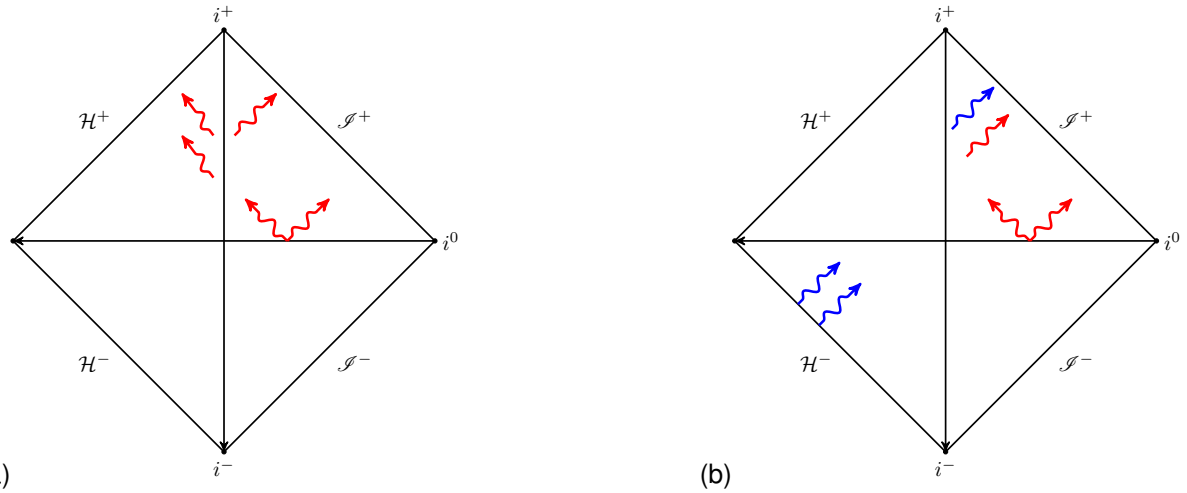

Figure 4.1: Carter-Penrose diagrams of the Schwarzschild region with the representations of the black hole (a) and WH (b) solutions for the Dirac delta potential. In (a), we see that the initial signal (red) reaches the potential, originating a dissipative term, which agrees with the quasinormal mode found for the BH. For (b), the difference in the boundary condition on the horizon becomes clear, as an impulse (blue) is emitted from the WH to cancel the part of the initial signal that is transmitted across the potential.

4.3 Poschl-Teller potential

In this case, one can begin from Eq. (4.4), now considering the Poschl-Teller potential, to obtain

$$\frac{d^2\Psi}{d^2r^*} + \left(\omega^2 - \frac{V_0}{\cosh^2\alpha(r_* - \bar{r}_*)}\right)\Psi = 0\,. \tag{4.29}$$

Here, $\bar{r}_*$ is the point where the potential reaches its maximum, with V_0 being the maximum value. It is easy to see that α has the property $\alpha^2 = (-2V_0)^{-1}d^2V/dr_*^2(\bar{r}_*)$. In this case, we impose the solutions to satisfy the following WH boundary conditions:

$$\begin{cases} \Psi \sim e^{-i\omega(t-r_*)} & , \quad r_* \to -\infty \quad (r \to r_h) \quad \text{(only outgoing at the horizon)} \\ \Psi \sim e^{-i\omega(t-r_*)} & , \quad r_* \to \infty \quad \text{(only outgoing at infinity in flat spacetime)} \end{cases} . \tag{4.30}$$

Here, the only difference for the BH case, is just the ingoing wave $e^{-i\omega(t+r_*)}$ at the horizon. To find the solution, we follow [24] where one starts by defining a new variable $\xi = \left(1 + e^{-2\alpha(r_* - \bar{r}_*)}\right)^{-1}$ that allows one to show that

$$\frac{1}{\cosh^2\alpha(r_* - \bar{r}_*)} = \frac{4e^{-2\alpha(r_* - \bar{r}_*)}}{\left(1 + e^{-2\alpha(r_* - \bar{r}_*)}\right)^2} = 4\xi(1-\xi)\,. \tag{4.31}$$

Then, with some algebra, one can write

$$\frac{d^2\xi}{dr_*^2} = -\left(e^{-4\alpha(r_* - \bar{r}_*)} - e^{-2\alpha(r_* - \bar{r}_*)}\right) = -4\alpha^2\xi(1-\xi)(2\xi - 1)\,, \tag{4.32}$$

as well as

$$\left(\frac{d\xi}{dr_*}\right)^2 = 4\alpha^2 e^{-4\alpha(r_*-\bar{r}_*)}\xi^4 = 4\alpha^2\xi^2(1-\xi)^2\,. \tag{4.33}$$

So, finally, using all these results, Eq. (4.29) takes the following form:

$$\xi^2(1-\xi)^2\frac{d^2\Psi}{d\xi^2} - \xi(1-\xi)(2\xi-1)\frac{d\Psi}{d\xi} + \left[\frac{\omega^2}{4\alpha^2} - \frac{V_0}{\alpha^2}\xi(1-\xi)\right]\Psi = 0\,. \tag{4.34}$$

It is also important to note that near spatial infinity $1-\xi \sim e^{-2\alpha(r_*-\bar{r}_*)}$ and near the horizon $\xi \sim e^{2\alpha(r_*-\bar{r}_*)}$. If we then define the variables $a = \left(\alpha + \sqrt{\alpha^2 - 4V_0} - 2i\omega\right)/(2\alpha)$, $b = \left(\alpha - \sqrt{\alpha^2 - 4V_0} - 2i\omega\right)/(2\alpha)$, $c = 1 - i\omega/\alpha$ and assume that the solution has the form $\Psi = (\xi(1-\xi))^{-i\omega/(2\alpha)}y$, we obtain a hypergeometric equation for y (see [25]):

$$\xi(1-\xi)\partial_\xi^2 y + [c - (a+b+1)\xi]\partial_\xi y - aby = 0\,. \tag{4.35}$$

The general solution for the hypergeometric equation is given by

$$\begin{aligned}\Psi =& A\xi^{i\omega/(2\alpha)}(1-\xi)^{-i\omega/(2\alpha)}F(a-c+1, b-c+1, 2-c, \xi) \\ &+ B(\xi(1-\xi))^{-i\omega/(2\alpha)}F(a,b,c,\xi)\,,\end{aligned} \tag{4.36}$$

where F is the hypergeometric function. Up to this point, we have still not imposed boundary conditions for neither a BH nor a WH. Let us first consider a BH, taking into account that $F(a_1, a_2, a_3, 0) = 1$ and that near the horizon $\xi^{i\omega/(2\alpha)} \sim e^{i\omega r_*}$, we see the first and second terms representing outgoing and ingoing waves, respectively. Therefore, BH boundary conditions require $A = 0$. To study the behaviour at infinity, one uses the $\xi \to 1-\xi$ transformation law for the hypergeometric function [25] to expand it, leading to

$$\begin{aligned}\Psi_{\text{BH}} = B\xi^{-i\omega/(2\alpha)}(1-\xi)^{-i\omega/(2\alpha)}\Bigg[&(1-\xi)^{i\omega/(\alpha)}\frac{\Gamma(c)\Gamma(a+b-c)}{\Gamma(a)\Gamma(b)}F(c-a, c-b, c-a-b+1, 1-\xi) \\ &+ \frac{\Gamma(c)\Gamma(c-a-b)}{\Gamma(c-a)\Gamma(c-b)}F(a,b,a+b-c+1,1-\xi)\Bigg]\,.\end{aligned} \tag{4.37}$$

Then, according to the boundary conditions at infinity, we have either $1/\Gamma(a) = 0$ or $1/\Gamma(b) = 0$, which leads to the existence of QNMs for BHs, given by

$$\omega_{\text{BH}} = \pm\sqrt{V_0 - \alpha^2/4} - i\alpha(2n+1)/2, \quad n = 0, 1, 2, \ldots\,. \tag{4.38}$$

Now, considering the WH, imposing (4.30), we can only have outgoing waves in the horizon in Eq. (4.36), which requires $B = 0$. The solution is then given by

$$\Psi_{\text{WH}} = A\xi^{i\omega/(2\alpha)}(1-\xi)^{-i\omega/(2\alpha)}F(a-c+1, b-c+1, 2-c, \xi)\,. \tag{4.39}$$

To study the behaviour at infinity, one uses the $\xi \to 1-\xi$ transformation law for the hypergeometric function to obtain the following result:

$$\begin{aligned}\Psi_{\text{WH}} =& A\xi^{i\omega/(2\alpha)}(1-\xi)^{-i\omega/(2\alpha)}\times \\ &\times\left[(1-\xi)^{i\omega/(\alpha)}\frac{\Gamma(2-c)\Gamma(a+b-c)}{\Gamma(a-c+1)\Gamma(b-c+1)}F(1-a,1-b,c-a-b+1,1-\xi)\right. \\ &\left.+\frac{\Gamma(2-c)\Gamma(c-a-b)}{\Gamma(1-a)\Gamma(1-b)}F(a-c+1,b-c+1,a+b-c+1,1-\xi)\right].\end{aligned} \tag{4.40}$$

When we consider the case for spatial infinity, we see that the term outside the parentheses becomes an outgoing wave, and the hypergeometric functions go to 1. According to the boundary conditions (4.30), we must ensure that the wave remains outgoing. Therefore, one must force the first term to go to 0 by imposing $1/\Gamma(a-c+1)=0$ or $1/\Gamma(b-c+1)=0$. However, in both arguments of the Gamma functions, ω vanishes. Although different approaches were also tried, the results were similar, once again showing that there are no quasinormal modes for this potential in the WH case.

5

QNMs of Schwarzschild spacetime

As mentioned earlier, the complexity of the equation described in (4.4) does not allow one to solve the wave equation analytically. After trying to use some toy models to emulate the potential and obtaining their solutions, we can now take a different approach. In this chapter, we shall try to use different numerical methods in order to calculate the quasinormal modes for the WH and compare them with the black hole results.

5.1 WKB approximation

Moving closer to the potential of Eq. (4.5), we can start by trying the Wentzel–Kramers–Brillouin (WKB) approximation. The procedure consists of dividing the potential into 3 regions, where the middle one is limited by the zeros of the function, $Q = \omega^2 - V(r)$. In the next figure, we show an example of a potential, where x_1 and x_2 denote the turning points, delimiting the 3 zones, and x_g the minimum or maximum, depending on the sign of the potential.

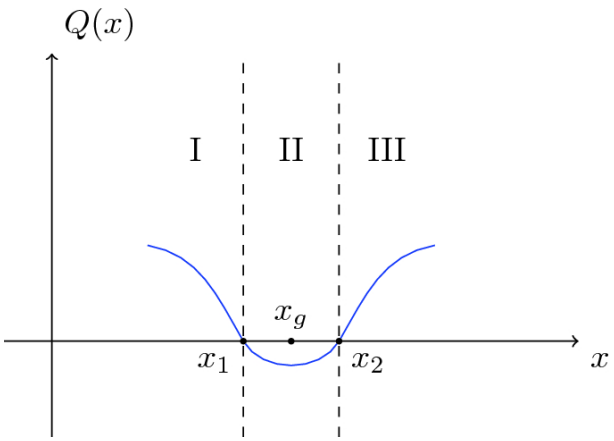

Figure 5.1: WKB method example for a negative potential [26]. With this figure becomes clear that for this approximation, the potential Q defined earlier is divide into three zones, delimited by the zeros of the function and centered in its minimum x_g.

Under these assumptions, we can apply this same method for our case by expanding Q in a Taylor series to the second order around the maximum $\bar{r}_*$ of the potential:

$$Q = \omega^2 - V \sim Q_0 + Q_0''(r_* - \bar{r}_*)^2/2\,. \tag{5.1}$$

Then by using this result in equation (4.4), it can be approximated to

$$\frac{d^2\Psi}{d^2r^*} + \left[Q_0 + \frac{1}{2}Q_0''(r_* - \bar{r}_*)^2\right]\Psi = 0\,. \tag{5.2}$$

This equation, describing zone II, possesses an exact solution in terms of the parabolic cylinder func-

tions, given by

$$\Psi = AD_\nu(z) + BD_{-\nu-1}(iz)\,, \quad \text{with} \quad z = (2Q_0'')^{\frac{1}{4}} e^{i\frac{\pi}{4}}(r_* - \bar{r}_*) \tag{5.3}$$

and $\nu = -iQ_0/\sqrt{2Q_0''} - 1/2$. Regarding conventions, for this subsection on the WKB method only, we will use the convention in [27], which, in a nutshell, reverses the signs on the exponentials. This was chosen so that one can compare both works more easily. For reference, we show the sign conventions in the following image:

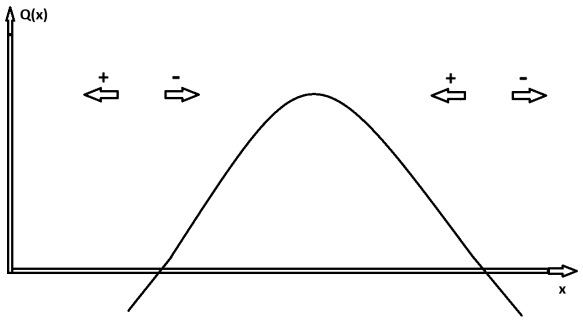

Figure 5.2: Illustrative graph of the function Q for Schwarzschild accompanied by the signal convention used in this subsection, which is contrary to the one used throughout the rest of the work.

Continuing the WKB method, it is important to note that the WKB solutions, outside the turning points, that is, in the zones I and III presented figuratively in Fig. 5.1, are given approximately by [27, 28]

$$\begin{aligned} \Psi_{III} &\approx Q^{-1/4} \exp\left(\pm i \int_{r_{2*}}^{r_*} [Q(t)]^{1/2} dt\right), \\ \Psi_I &\approx Q^{-1/4} \exp\left(\pm i \int_{r_*}^{r_{1*}} [Q(t)]^{1/2} dt\right). \end{aligned} \tag{5.4}$$

Focusing on these integrals, with $Q(t)$ given by (5.1), one can denote $\sqrt{Q(t)}$ as the derivative of $F(t)$, and so

$$\int_{r_*}^{r_{1*}} [Q(t)]^{1/2} dt = \int_{r_*}^{r_{1*}} \frac{dF}{dt} dt = [F(r_{1*}) - F(r_*)]\,. \tag{5.5}$$

According to equation (5.4), this result allows to state that

$$\begin{aligned} \Psi_I^{\text{WH}} &\approx Q^{-1/4} \exp\left(\pm i\left[F(r_{1*}) - F(r_*)\right]\right) \propto Q^{-1/4} \exp\left(\mp i F(r_*)\right) \xrightarrow{B.C.} Q^{-1/4} \exp\left(i F(r_*)\right), \\ \Psi_I^{\text{BH}} &\approx Q^{-1/4} \exp\left(\pm i\left[F(r_{1*}) - F(r_*)\right]\right) \propto Q^{-1/4} \exp\left(\mp i F(r_*)\right) \xrightarrow{B.C.} Q^{-1/4} \exp\left(-i F(r_*)\right), \\ \Psi_{III} &\approx Q^{-1/4} \exp\left(\pm i\left[F(r_*) - F(r_{2*})\right]\right) \propto Q^{-1/4} \exp\left(\pm i F(r_*)\right) \xrightarrow{B.C.} Q^{-1/4} \exp\left(-i F(r_*)\right). \end{aligned} \tag{5.6}$$

By examining the difference in the solutions for both zones, one can conclude that, for zone I, the exponentials have the opposite signal. This implies that one must kill the term with the negative signal to obey the WH boundary conditions, and the opposite for the BH case. To look at the behaviour in spatial infinity and in the horizon, we used the asymptotic expansion of the parabolic cylinder [27], with the results for $r_* \to +\infty$ given by

$$\Psi \sim Be^{-3i\pi(\nu+1)/4} z^{-(\nu+1)} e^{z^2/4} + \left(A + B\frac{\sqrt{2\pi}}{\Gamma(\nu+1)} e^{-i\pi(\nu+1)/2} \right) z^{\nu} e^{-z^2/4}\,, \tag{5.7}$$

and for $r_* \to -\infty$

$$\Psi \sim Ae^{-3i\pi\nu/4} z^{\nu} e^{-z^2/4} + \left(B + A\frac{\sqrt{2\pi}}{\Gamma(-\nu)} e^{-i\pi\nu/2} \right) z^{-(\nu+1)} e^{z^2/4}\,. \tag{5.8}$$

Looking first to the case of the BH, the exponentials $e^{-z^2/4}$ in Eqs. (5.7,5.8) represent the waves moving away from the potential; therefore, the boundary conditions require $B = 0$ and $\Gamma(-\nu) = 0$. This last condition implies that

$$\frac{Q_0}{\sqrt{2Q_0''}} = -i\,(n + 1/2)\,, \quad n = 0, 1, 2, \ldots\,. \tag{5.9}$$

Having reached this result, we can apply it in equations (4.4) and (4.5), where we can use [27] notation to write the equation in a more general case, including the three types of perturbation:

$$\left[\frac{d^2}{d^2 r^*} + \omega^2 - f(r) \left(\mu^2 + \frac{l(l+1)}{r^2} + (1 - s^2)\frac{2M}{r^3} \right) \right] R(r) = 0\,, \tag{5.10}$$

with l being the angular harmonic index. According to our definition of Q, we have

$$\begin{aligned} Q' =& 2M\mu^2 \left(\frac{1}{r^2}\right) - 2\lambda \left(\frac{1}{r^3}\right) - 6M(1 - s^2 - \lambda)\mu^2 \left(\frac{1}{r^4}\right) + 16M^2(1 - s^2) \left(\frac{1}{r^5}\right), \\ Q'' =& -4M\mu^2 \left(\frac{1}{r^3}\right) + 6\lambda \left(\frac{1}{r^4}\right) + 24M(1 - s^2 - \lambda)\mu^2 \left(\frac{1}{r^5}\right) - 80M^2(1 - s^2) \left(\frac{1}{r^6}\right), \end{aligned} \tag{5.11}$$

with $\lambda = l(l+1)$. In order to simplify the calculations and avoid cubic equations, we can consider μ to be 0. In this case, the extremal point of $-Q$ is given by $r = r_0 = \frac{3M}{2\lambda}(\lambda - 1 + s^2 + [\lambda^2 + (1 - s^2)^2 + (14/9)\lambda(1 - s^2)]^{1/2})$. Then, by using Eq. (5.9) with radial coordinates in units of M, we have

$$\omega^2 = f(r_0) \left(\frac{\lambda}{r_0^2} + \frac{2(1 - s^2)}{r_0^3} \right) - i\sqrt{2Q_0''}(n + \frac{1}{2})\,. \tag{5.12}$$

In the following tables, we present the frequency results for the fundamental modes ($n = 0$), with units of $M = 1$, and for the three different types of perturbations, which agree perfectly with [27]:

l	Re ω	Im ω
2	0.399	−0.0883
3	0.617	−0.0923
4	0.822	−0.0939

Table 5.1: Quasinormal modes imaginary and real parts computed using the WKB approximation for the Schwarzschild black hole for gravitational perturbations ($s = \pm 2$).

l	Re ω	Im ω
2	0.506	−0.0961
3	0.692	−0.0961
4	0.880	−0.0962

Table 5.2: Quasinormal modes imaginary and real parts computed using the WKB approximation for the Schwarzschild black hole for scalar perturbations ($s = 0$).

l	Re ω	Im ω
2	0.481	−0.0944
3	0.673	−0.0953
4	0.866	−0.0956

Table 5.3: Quasinormal modes imaginary and real parts computed using the WKB approximation for the Schwarzschild black hole for electromagnetic perturbations ($s = \pm 1$).

Considering now the WH case, if we look first at (5.8) and considering that, by the boundary conditions, the term $e^{z^2/4}$ is proportional to the outgoing terms in (5.6), then, since we only want outgoing terms in horizon, A must be 0. This conditions leads to Eq. (5.7) to have the following form

$$\Psi \sim Be^{-3i\pi(\nu+1)/4} z^{-(\nu+1)} e^{z^2/4} + B\frac{\sqrt{2\pi}}{\Gamma(\nu+1)} e^{-i\pi(\nu+1)/2} z^{\nu} e^{-z^2/4}. \tag{5.13}$$

Again, since we only want to keep the $e^{-z^2/4}$ term, now proportional to the outgoing wave, we have that $B = 0$. Therefore, we show that through WKB, it is not possible to obtain quasinormal modes for the WH.

5.2 Direct integration

In this section, we will try to use the direct integration method in equation (4.4) in order to numerically obtain the quasinormal modes of a black and white hole. This will be done using Mathematica, and we will use a similar method used by Chandrasekhar and Detweiler [29]. The code starts by defining our equation and variables using the nomenclature in [30], considering the case of 4 dimensions to recover equations (4.4) and (4.5), but we will use gravitational and scalar perturbations to compare the accuracy of this code with other works.

After carefully defining our setup, we proceed to obtain a series near the event horizon limit. In this series, we impose a purely ingoing or outgoing wave boundary condition, depending on whether we are in the BH or WH case, using the ansatz

$$\Psi = (r - r_h)^{\mp i\omega r_h} \sum_{n=0}^{\infty} h_n (r - r_h)^n \quad \text{with} \quad r_h = 2M\,. \tag{5.14}$$

After obtaining the series, the same process is performed for the large distance limit (that is, near infinity), in order to obtain an approximate solution for both limits of r. For this limit, we use the ansatz

$$\Psi = e^{i\omega r_*} \sum_{n=0}^{\infty} \frac{g_n}{r^n}. \tag{5.15}$$

This ansatz implies a totally outgoing wave as a boundary condition, as required in both cases. For both series, it was necessary to include at least 10 orders to obtain stability.

The next step is to define a function, which we denote as INT, to perform an integration, divided into two parts. After receiving the parameters, one can first use the horizon series to define the equation and the boundary conditions to integrate it using the function "NDSolve" from the horizon to a matching point, which we denote as r_m. Subsequently, the same is done for the infinity series, integration from r_m to a sufficiently large distance defined by the user. Then, a linear combination of the two solutions is constructed, and we fix the ratio of the coefficients for the linear combination to be $\mathcal{C}^0$. Finally, the INT function receives the parameters (r_m, l, ϵ and infinity value) and returns the jump of the first derivative at r_m for a given ω. Here, the infinity value is just a sufficiently large distance and ϵ is just a residual value that is added in the integration to avoid errors during the calculations at the horizon.

Ultimately, to obtain the quasinormal modes, we use the expression returned by the function INT and search for ω in order for the first derivative to be continuous. To do this, we use the function "FindRoot", using an initial guess for the values of the quasinormal modes. Finally, we obtain the result for ω and calculate the absolute value of the expression returned by the function INT, using the value of ω obtained. This value is denoted as residue; since its expression represents the condition for the derivative to be continuous, it indicates how good that value ω is, depending on how close it is to zero. Then both ω and residue values are presented, allowing us to understand the quality of the quasinormal mode obtained. Due to the units used in the compared works, we have set $2M = 1$ for gravitational perturbations and $M = 1$ for the scalar perturbations.

To test the precision of our results, we compared them with the values for the black hole quasinormal modes in [31], for the gravitational perturbation case. As mentioned earlier, one has to provide an initial guess for ω. Regarding the first modes with $n = 1, 2$ and $l = 2$, the code was able to reach good precision with a less precise guess. However, for the rest, one had to give much less precise guesses to obtain a result, but still avoid previous modes. In the following tables, we present the results obtained

from this comparison.

	Results		Ref. [31]		$\delta(\%)$	
n	Re ω	Im ω	Re ω	Im ω	Re	Im
1	0.747343	-0.177925	0.747343	-0.177925	0	0
2	0.699995	-0.540018	0.693422	-0.547830	0.95	1.43

Table 5.4: Quasinormal modes imaginary and real parts in $2M = 1$ units, computed using the direct integration numerical method for the Schwarzschild black hole for gravitational perturbations for $l = 2$. The values are then compared with [31] trough their deviation.

	Results		Ref. [31]		$\delta(\%)$	
n	Re ω	Im ω	Re ω	Im ω	Re	Im
1	1.19889	-0.185406	1.198887	-0.185406	2.5×10^{-4}	0
2	1.10005	-0.560173	1.165288	-0.562596	5.6	0.43

Table 5.5: Quasinormal modes imaginary and real parts in $2M = 1$ units, computed using the direct integration numerical method for the Schwarzschild black hole for gravitational perturbations for $l = 3$. The values are then compared with [31] trough their deviation.

After comparing these results, it becomes clear that this method can indeed produce good results to some extent. For the first quasinormal modes for $l = 2$ and $l = 3$, the results are very satisfying, with practically no difference from the reference results. However, as one looks for modes for higher n, the errors start to grow. For both $l = 2$ and $l = 3$ there was no sufficiently small initial guess that would not lead to previous modes in $n = 3$ or lead to incorrect values or errors with the "FindRoot" function. In the case of $n = 2$, some of the parameters had to be altered compared to $n = 1$ to obtain satisfactory results. Finally, one can conclude that this code seems to produce good results for the first modes, but higher order modes will not be pursued in further sections, since it leads to either wrong results or no convergence.

We conducted a similar study for the scalar case, where we now compared our results with those in [32]. In this case, l took the values of 0, 1 and 2, and, for each first mode $n = 0$, the accuracy was very satisfying. However, for the rest of the values of n, it was not possible to obtain reliable results, due to errors in the calculation. In the following tables, we present the results of the comparison.

	Direct Integration		Ref. [32]		$\delta(\%)$	
l	Re ω	Im ω	Re ω	Im ω	Re	Im
0	0.1103	-0.1042	0.1105	-0.1049	0.16	0.65
1	0.2929	-0.0977	0.2929	-0.0977	0	0
2	0.4836	-0.0968	0.4836	-0.0968	0	0

Table 5.6: Quasinormal modes imaginary and real parts in $M = 1$ units, computed using the direct integration numerical method for the Schwarzschild black hole for scalar perturbations for $n = 0$. The values are then compared with [32] trough their deviation.

Once again, the table shows that the code can indeed produce very good and precise results when

comparing these quasinormal modes. For the first overtones, it is clear that this code produces very satisfactory results. However, compared to the gravitational case, it was not able to find other modes inside the multipole. Despite trying different guesses, it was not possible to converge or even obtain results without errors occurring in the "FindRoot" function for other modes than those presented in the table. Nevertheless, for the first overtones, this method has shown very promising and accurate results; our future research will take that into account. To test how the parameters of the function influenced the results, we analyzed those variables, presented in the Appendix C. The objective here was to study the quality of our numerical values when varying each parameter separately. This allowed us to find the optimal range for each parameter, in order to obtain the best possible results for the future possible quasinormal modes that one can calculate.

5.3 White hole QNMs

As we have mentioned in earlier sections, to obtain the QNMs for the WH we have to change the boundary condition at the horizon. This change consists in imposing a purely outgoing wave at the horizon and maintaining a purely outgoing wave at infinity as well. The modes for these specific boundary conditions have already been considered in the literature, and are denoted as "left"-total transmission modes (TTM$_L$s). Analogously, if one keeps the boundary condition at the horizon as purely ingoing, and at infinity we also impose purely ingoing, we have "right"-total transmission modes (TTM$_R$s).

These total transmission modes (TTMs) were first considered for the Kerr spacetime, in the context of algebraically special modes, by Wald [33] and in more detail by Chandrasekhar [34]. In general, for Kerr, these and other modes have to be determined using analytical approximations or numerically, with [35, 36] shedding light on those results and theory. Fortunately, for the Schwarzschild limit $a = 0$, the TTMs and their complex frequencies can be determined analytically. For this case, with gravitational perturbations, the frequencies take on the purely imaginary values

$$\Omega_l = -\frac{i}{12}(l-1)l(l+1)(l+2)\,. \tag{5.16}$$

These TTM$_L$s have in fact been considered to be applied exclusively to black holes. Our proposal in this work is to instead consider these modes as being the QNMs of a WH. In fact, Maassen van den Brink [37] has rigorously proven that, for Schwarzschild, the modes Ω_l are simultaneously QNMs and TTM$_L$s, but not TTM$_R$s. Therefore, this could be an argument in favor of our proposal. Since all these modes are, in fact, calculated purely for the Schwarzschild spacetime, instead of assuming that all of them belong to a BH, one can, through the boundary conditions, attribute these quasinormal modes to a specific object. Accordingly, since Ω_l are simultaneously QNMs and TTM$_L$s, these can instead still be QNMs, in Schwarzschild, but for the WH. Due to the purely imaginary nature of these modes, the

evidence for stability becomes clear for WHs in this case. The exponential possesses no oscillatory terms, which leads to a smooth and purely exponential decay of the intensity's signal with time. This shows that there is indeed stability in the WH system when applying gravitational perturbations.

In relation to the results obtained by direct integration, unfortunately, they were not satisfactory. After fully adapting the code, and looking for results, we have only found two viable values. Eventhough both were practically on the negative imaginary axis, neither of them presented strong enough convergence or compatible behaviours, and the rest of the results were even worse in these aspects. It was also not possible to obtain acceptable values when looking for the modes in (5.16). In other words, direct integration is not suitable to numerically determine purely imaginary QNMs expected for the WH. Despite the fact one can obtain them analitically, it would be of interest to find them numerically or semi-analytically. It is also important to note that, from this point of view, the modes presented in (5.16), do not agree with the results obtained in Ref. [38].

6

Conclusions

The main motivation for this work was to study the WH carefully, providing a basic setup for its formation, evolution, and dynamics. The WH, which has not received a lot of attention, is a very exotic and interesting object with the potential to help us understand black holes and our universe, making it important to further understand it.

We started by reviewing the maximal analytical solution for the Schwarzschild WH and the construction of the corresponding Carter-Penrose diagram, and also calculated the surface gravity for the WH. To address the formation and evolution of this object, it was necessary to consider a time-reversed Oppenheimer-Snyder collapse through a matching perspective. To do this, a careful study of the FLRW model was made, and the Friedman equation was obtained. Through the matching of the FLRW and Schwarzschild-de Sitter metrics, we obtained a new solution to Einstein's field equations. Taking the cosmological constant to be zero, by simplicity, after reversing and redefining our time parameter, we were able to obtain the Carter-Penrose diagrams for the WH solutions originating from a time-reversed Oppenheimer-Snyder collapse. This made it possible to understand the different evolutions of the WH. For $k = 0\,, -1$ (where k is the spatial curvature parameter of the FLRW solution), we have a dust sphere coming out of the singularity, crossing the horizon, and radially expanding indefinitely. In the more interesting case, for $k = 1$, we have the dust sphere exiting the WH, expanding until it reaches a maximum radius, and then recollapsing into a black hole. Showing the existence of this solution is of the utmost importance, since it solves two major challenges of a WH: the absence of a confirmed detection and the non-stop emission of matter and radiation. The recollapse into a black hole revives the possibility of existence for these objects and adds a greater complexity and depth to their evolution.

In the second part of this thesis, we were interested in studying the dynamics of the WH in Schwarzschild. Our main objective was to carefully build a rigorous and solid basis for studying the stability of this object, given the absence of relevant information in the literature. To do this, we studied the quasinormal modes of a WH, starting by obtaining the wave equation for a scalar field in Schwarzschild. The crucial difference in comparison with the black hole case is the boundary condition at the horizon, where it was imposed to have only outgoing waves. Starting by using a semi-analytical approach, we tried to obtain the QNMs for selected potentials, Dirac delta and Poschl-Teller, finishing with the WKB approximation. For these three cases, we found that there were no quasinormal modes, but it was still possible to find the solutions to the equations of motion for some cases, always making a parallel with the black hole case. We also made a more in-depth analysis and interpretation of the Dirac delta solution, where it was possible to understand the weird behaviour and interactions of the solutions.

By proceeding to use a numerical technique, the direct integration method was chosen to calculate the QNMs of Schwarzschild spacetime, both for black and WHs. We started by studying the quality of the results for the black hole case, using different types of perturbations. To a certain degree, the values obtained were very satisfactory when compared with the literature. To improve these results, a

parameter analysis was made to determine the best interval of initial values leading to the best precision possible. Through a thorough review of the literature, it was clear that modes calculated for the WH boundary conditions do exist, and are called left total transmission modes. These also exist in the Schwarzschild limit and can be obtained analytically for this case. In this thesis, we argue, for the first time, that these QNMs should be considered not as black hole QNMs, but rather as WH QNMs. Following this argument, we concluded there can be stability in the WH system, as the QNMs decay exponentially with time. Unfortunately, due to the purely imaginary nature of these modes, the results from the direct integration method were not satisfactory, and it was not possible to obtain convergence for those values.

Besides the work already presented for the dynamics of the WH, there are many other aspects that should be further studied. The use of other numerical methods, such as the continued fraction method, can also be used in order to successfully obtain the QNMs for the Schwarzschild WH. It is also important to make a more complete study of the recollapse solution and its dynamics. Such work may help uncover the potential of this interesting evolution and shed some light on WHs. These and other aspects show that the research on the WH is far from over, and further work is essential.

Bibliography

[1] *Scharzschild Carter-Penrose diagram*. https://tikz.net/relativity_penrose_diagram/. Accessed: 2025-10-31.

[2] Jakob Hansen. “Evolution Problems of General Relativity”. PhD thesis. Niels Bohr Institute, 2005.

[3] *Kerr Carter-Penrose diagram*. https://jila.colorado.edu/~ajsh/insidebh/penrose.html. Accessed: 2025-10-31.

[4] Roger Penrose. “Gravitational collapse: The role of general relativity”. In: *Riv. Nuovo Cim.* 1 (1969), pp. 252–276.

[5] Charles W Misner, Kip S Thorne, and John Archibald Wheeler. *Gravitation*. Macmillan, 1973.

[6] J Robert Oppenheimer and Hartland Snyder. “On continued gravitational contraction”. In: *Physical Review* 56.5 (1939), p. 455.

[7] Charlie Rose. “A Conversation with Dr. Stephen Hawking and Lucy Hawking”. In: *charlierose. com* (2013).

[8] Richard Brito, Vitor Cardoso, and Paolo Pani. “Superradiance–the 2020 Edition”. In: *arXiv preprint arXiv:1501.06570* (2015).

[9] CV Vishveshwara. “Scattering of gravitational radiation by a Schwarzschild black-hole”. In: *Nature* 227.5261 (1970), pp. 936–938.

[10] Alon Retter and Shlomo Heller. “The revival of white holes as Small Bangs”. In: *New Astronomy* 17.2 (2012), pp. 73–75.

[11] Rudeep Gaur and Matt Visser. “Black holes, white holes, and near-horizon physics”. In: *Journal of High Energy Physics* 2024.5 (2024), pp. 1–19.

[12] Eugenio Bianchi et al. “White holes as remnants: a surprising scenario for the end of a black hole”. In: *Classical and Quantum Gravity* 35.22 (2018), p. 225003.

[13] Nikodem J Popławski. “Radial motion into an Einstein–Rosen bridge”. In: *Physics Letters B* 687.2-3 (2010), pp. 110–113.

[14] Kayll Lake. “White holes”. In: *Nature* 272.5654 (1978), pp. 599–601.

[15] Douglas M Eardley. “Death of white holes in the early universe”. In: *Physical Review Letters* 33.7 (1974), p. 442.

[16] JV Narlikar, KMV Appa Rao, and Naresh Dadhich. “High energy radiation from white holes”. In: *Nature* 251.5476 (1974), pp. 590–591.

[17] Claude Barrabès, Patrick R Brady, and Eric Poisson. “Death of white holes”. In: *Physical Review D* 47.6 (1993), p. 2383.

[18] Steven K Blau. “Dray–’t Hooft geometries and the death of white holes”. In: *Physical Review D* 39.10 (1989), p. 2901.

[19] Ray d’Inverno and James Vickers. *Introducing Einstein’s relativity: a deeper understanding*. Oxford University Press, 2022.

[20] José Natário. *Mathematical relativity*. 2020. arXiv: 2003.02855 [gr-qc]. URL: https://arxiv.org/abs/2003.02855.

[21] Eric Poisson. *A relativist’s toolkit: the mathematics of black-hole mechanics*. Cambridge university press, 2004.

[22] Helvi Witek et al. “Superradiant instabilities in astrophysical systems”. In: *Physical Review D—Particles, Fields, Gravitation, and Cosmology* 87.4 (2013), p. 043513.

[23] R Brito. “Dynamics around black holes: radiation emission and tidal effects,(2012)”. In: *arXiv preprint arXiv:1211.1679* (2012).

[24] Emanuele Berti, Vitor Cardoso, and Andrei O Starinets. “Quasinormal modes of black holes and black branes”. In: *Classical and Quantum Gravity* 26.16 (July 2009), p. 163001. ISSN: 1361-6382. DOI: 10.1088/0264-9381/26/16/163001. URL: http://dx.doi.org/10.1088/0264-9381/26/16/163001.

[25] Milton Abramowitz. *Handbook of Mathematical Functions, With Formulas, Graphs, and Mathematical Tables,* USA: Dover Publications, Inc., 1974. ISBN: 0486612724.

[26] Black Holes. “WKB Method and Quasinormal Modes of String-Theoretical D-Dimensional”. In: *Compact Objects in the Universe* (2024), p. 203.

[27] Bernard F Schutz and Clifford M Will. “Black hole normal modes: a semianalytic approach”. In: *The Astrophysical Journal* 291 (1985), pp. L33–L36.

[28] Carl M Bender and Steven A Orszag. *Advanced mathematical methods for scientists and engineers I: Asymptotic methods and perturbation theory*. Springer Science & Business Media, 2013.

[29] Subrahmanyan Chandrasekhar and Steven Detweiler. “The quasi-normal modes of the Schwarzschild black hole”. In: *Proceedings of the Royal Society of London. A. Mathematical and Physical Sciences* 344.1639 (1975), pp. 441–452.

[30] Vitor Cardoso, José P. S. Lemos, and Shijun Yoshida. “Quasinormal modes of Schwarzschild black holes in four and higher dimensions”. In: *Physical Review D* 69.4 (Feb. 2004). ISSN: 1550-2368. DOI: 10.1103/physrevd.69.044004. URL: http://dx.doi.org/10.1103/PhysRevD.69.044004.

[31] Edward W Leaver. “An analytic representation for the quasi-normal modes of Kerr black holes”. In: *Proceedings of the Royal Society of London. A. Mathematical and Physical Sciences* 402.1823 (1985), pp. 285–298.

[32] RA Konoplya. “Quasinormal modes of the Schwarzschild black hole and higher order WKB approach”. In: *J. Phys. Stud* 8.93 (2004), p. 80.

[33] Robert M. Wald. “On perturbations of a Kerr black hole”. In: *J. Math. Phys.* 14.10 (1973), pp. 1453–1461. DOI: 10.1063/1.1666203.

[34] Subrahmanyan Chandrasekhar. “On algebraically special perturbations of black holes”. In: *Proceedings of the Royal Society of London. A. Mathematical and Physical Sciences* 392.1802 (1984), pp. 1–13.

[35] Gregory B Cook and Maxim Zalutskiy. “Gravitational perturbations of the Kerr geometry: High-accuracy study”. In: *Physical Review D* 90.12 (2014), p. 124021.

[36] Gregory B Cook and Maxim Zalutskiy. “Modes of the Kerr geometry with purely imaginary frequencies”. In: *Physical Review D* 94.10 (2016), p. 104074.

[37] Alec Maassen van den Brink. “Analytic treatment of black-hole gravitational waves at the algebraically special frequency”. In: *Physical Review D* 62.6 (2000), p. 064009.

[38] Nigel T Bishop and Amos S Kubeka. “Quasinormal modes of a Schwarzschild white hole”. In: *Physical Review D—Particles, Fields, Gravitation, and Cosmology* 80.6 (2009), p. 064011.

[39] Nigel T Bishop et al. “High-powered gravitational news”. In: *Physical Review D* 56.10 (1997), p. 6298.

[40] Nigel T Bishop. “Linearized solutions of the Einstein equations within a Bondi–Sachs framework, and implications for boundary conditions in numerical simulations”. In: *Classical and Quantum Gravity* 22.12 (2005), p. 2393.

[41] Christian Reisswig et al. “Characteristic evolutions in numerical relativity using six angular patches”. In: *Classical and Quantum Gravity* 24.12 (2007), S327.

[42] Christian Reisswig et al. “Characteristic extraction in numerical relativity: binary black hole merger waveforms at null infinity”. In: *Classical and quantum gravity* 27.7 (2010), p. 075014.

[43] Roberto Gómez et al. “The eth formalism in numerical relativity”. In: *Classical and Quantum Gravity* 14.4 (1997), p. 977.

[44] Ezra T Newman and Roger Penrose. “Note on the bondi-metzner-sachs group”. In: *Journal of Mathematical Physics* 7.5 (1966), pp. 863–870.

[45] Joshua N Goldberg et al. “Spin-s Spherical Harmonics and ”. In: *Journal of Mathematical Physics* 8.11 (1967), pp. 2155–2161.

A

Fundamental equations

$$R_{\mu\nu} = \partial_\rho \Gamma^\rho_{\mu\nu} - \partial_\mu \Gamma^\rho_{\nu\rho} + \Gamma^\rho_{\rho\lambda}\Gamma^\lambda_{\mu\nu} - \Gamma^\rho_{\mu\lambda}\Gamma^\lambda_{\rho\nu}\,. \tag{A.1}$$

$$\Gamma^\alpha_{\mu\nu} = \frac{1}{2} g^{\alpha\lambda}(\partial_\nu g_{\lambda\mu} + \partial_\mu g_{\lambda\nu} - \partial_\lambda g_{\mu\nu})\,. \tag{A.2}$$

B

Mathematical Lemmas

B.1 Lemma 1

Let (M, g) be a Riemannian or a Lorentzian manifold and $S \subset M$ a hypersurface whose normal vector field n satisfies $g(n, n) \neq 0$. The hypersurfaces S_t obtained from S by moving a distance t along the geodesics orthogonal to S remain orthogonal to the geodesics.

B.2 Lemma 2

Let (M, g) be a Riemannian or a Lorentzian manifold and $p \in M$. The hypersurfaces S_t obtained from p by moving a distance t along the geodesics through p remain orthogonal to the geodesics.

C

Parameter analysis

To test how the parameters of the function INT influenced the results, we decided to use the overtones of $l = 2, 3$ for the gravitational case, and $l = 1, 2$ for the scalar case due to the better precision obtained. One of the parameters is the matching point, denoted as r_m, where we evaluate the derivative. This point is where we match both integrations of the horizon and infinity series, representing the maximum and minimum limits of the integral respectively. Another parameter is the infinity, which is just a sufficiently large value for the limit of the inifinity series integration. Finally we are left with the parameter ϵ that is just a residual value added to the horizon limit to avoid singularities errors. The usual values used were 20, 10 and 10^{-4}, for r_m, infinity and ϵ respectively, and those should be assumed unless said otherwise. The value for r_m was chosen to be almost equally distant from both the horizon and infinity. Taking into account that for the overtones the results were very stable, we will analyse the residue value so that, for each variation of each parameter, we find the optimal range to obtain the best quality possible for the results. Then, for each of these 3 parameters, we will see how the absolute value changes with each parameter variation, as long as no errors occur, allowing us to understand the optimal range for these parameters. In the following tables, we present the matching point analysis, where the values of ω have remained stable and equal to (5.4,5.5) for gravitational perturbation, and to (5.6) in the scalar case.

C.1 Matching point analysis

C.1.1 Gravitational perturbation

r_m	Residue	r_m	Residue
2	9.7×10^{-11}	11	8.5×10^{-13}
3	4.4×10^{-11}	12	4.6×10^{-13}
4	1.3×10^{-11}	13	4.1×10^{-13}
5	9.5×10^{-12}	14	1.3×10^{-13}
6	8.4×10^{-12}	15	2.6×10^{-13}
7	4.1×10^{-12}	16	3.9×10^{-14}
8	3.7×10^{-12}	17	8.4×10^{-14}
9	1.8×10^{-12}	18	6.4×10^{-14}
10	4.4×10^{-13}	19	4.1×10^{-14}

Table C.1: Residue value evolution for different values of the matching point, in a Schwarzschild black hole for a gravitational perturbation, using the direct integration numerical method, for $l = 2$.

r_m	Residue	r_m	Residue
2	1.96×10^{-10}	11	4.4×10^{-13}
3	1.9×10^{-11}	12	4.3×10^{-13}
4	4.2×10^{-11}	13	4.8×10^{-13}
5	8.5×10^{-12}	14	1.9×10^{-13}
6	1.4×10^{-11}	15	2.2×10^{-13}
7	5.3×10^{-12}	16	4.94×10^{-14}
8	1.02×10^{-12}	17	1.9×10^{-13}
9	2.2×10^{-12}	18	7.3×10^{-14}
10	6.8×10^{-13}	19	5.2×10^{-14}

Table C.2: Residue value evolution for different values of the matching point, in a Schwarzschild black hole for a gravitational perturbation, using the direct integration numerical method, for $l = 3$.

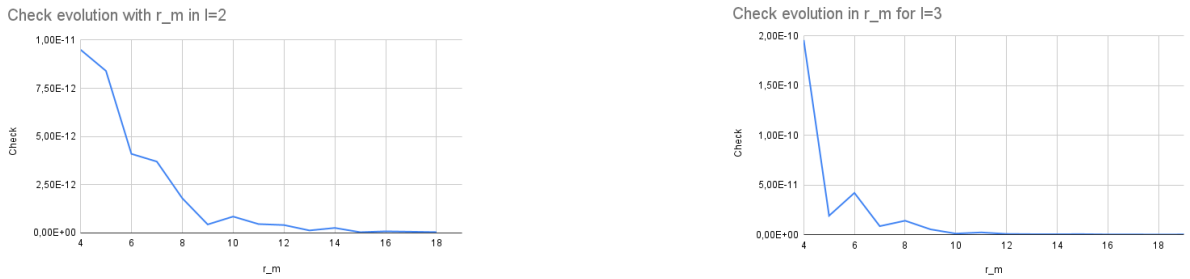

Figure C.1: Residue value evolution for different values of the matching point, in a Schwarzschild black hole for a gravitational perturbation, using the direct integration numerical method, for $l = 2$ and $l = 3$.

C.1.2 Scalar perturbation

r_m	Residue	r_m	Residue
2	–	11	1.1×10^{-11}
3	7.5×10^{-10}	12	2.3×10^{-12}
4	–	13	3.9×10^{-12}
5	3.2×10^{-11}	14	3.5×10^{-12}
6	4.4×10^{-11}	15	5.9×10^{-12}
7	2.0×10^{-11}	16	1.3×10^{-12}
8	–	17	1.5×10^{-12}
9	7.1×10^{-11}	18	2.6×10^{-12}
10	3.3×10^{-12}	19	4.3×10^{-13}

Table C.3: Residue value evolution for different values of the matching point, in a Schwarzschild black hole for a scalar perturbation, using the direct integration numerical method, for $l = 1$.

r_m	Residue	r_m	Residue
2	–	11	6.7×10^{-12}
3	9.7×10^{-10}	12	2.5×10^{-12}
4	1.4×10^{-10}	13	3.9×10^{-12}
5	9.7×10^{-11}	14	4.5×10^{-12}
6	9.4×10^{-12}	15	4.8×10^{-12}
7	3.9×10^{-11}	16	1.0×10^{-12}
8	9.3×10^{-12}	17	1.7×10^{-12}
9	8.0×10^{-12}	18	1.7×10^{-12}
10	1.2×10^{-11}	19	1.0×10^{-12}

Table C.4: Residue value evolution for different values of the matching point, in a Schwarzschild black hole for a scalar perturbation, using the direct integration numerical method, for $l = 2$.

Figure C.2: Residue value evolution for different values of the matching point, in a Schwarzschild black hole for a scalar perturbation, using the direct integration numerical method, for $l = 2$ and $l = 3$.

The evolution with the matching point is quite clear, with a significant decrease as we move r_m closer to the designated ”infinity”. However, after the matching point reaches values of 10/11, there is some stabilization, and a final decrease for the infinity limit. In terms of optimal values for r_m, the region 10 to 14 seems to be the most suitable, where we have fewer oscillations, in order to assure stability.

C.2 Epsilon analysis

The following analysis presents the evolution of the residue value with the parameter ϵ going from 10^{-1} to 10^{-10}. For some of these values, there was also a difference in ω, so it was decided to present those values for all the cases.

C.2.1 Gravitational perturbation

ϵ	Residue	ω	ϵ	Residue	ω
10^{-1}	3.2×10^{-14}	$0.747343 - 0.177925i$	10^{-1}	6.6×10^{-14}	$1.19889 - 0.185406i$
10^{-2}	5.8×10^{-14}	$0.747343 - 0.177925i$	10^{-2}	1.9×10^{-13}	$1.19889 - 0.185406i$
10^{-3}	6.4×10^{-15}	$0.747343 - 0.177925i$	10^{-3}	1.2×10^{-13}	$1.19889 - 0.185406i$
10^{-4}	4.4×10^{-13}	$0.747343 - 0.177925i$	10^{-4}	6.8×10^{-13}	$1.19889 - 0.185406i$
10^{-5}	6.1×10^{-12}	$0.747343 - 0.177925i$	10^{-5}	2.2×10^{-12}	$1.19889 - 0.185406i$
10^{-6}	5.1×10^{-11}	$0.747343 - 0.177925i$	10^{-6}	3.2×10^{-11}	$1.19889 - 0.185406i$
10^{-7}	–	–	10^{-7}	1.3×10^{-10}	$1.19889 - 0.185406i$
10^{-8}	–	–	10^{-8}	–	–
10^{-9}	–	–	10^{-9}	2.01×10^{-12}	$0.107376 - 0.227515i$
10^{-10}	3.4×10^{-14}	$0.048325 - 0.194419i$	10^{-10}	7.1×10^{-13}	$0.107376 - 0.227515i$

Table C.5: Residue value evolution for different values of the ϵ, in a Schwarzschild black hole for a gravitational perturbation, using the direct integration numerical method, for $l = 2$ (left) and $l = 3$ (right).

C.2.2 Scalar perturbation

ϵ	Residue	ω	ϵ	Residue	ω
10^{-1}	1.1×10^{-12}	$0.292936 - 0.09766i$	10^{-1}	7.2×10^{-13}	$0.483644 - 0.0967588i$
10^{-2}	1.2×10^{-12}	$0.292936 - 0.09766i$	10^{-2}	8.5×10^{-13}	$0.483644 - 0.0967588i$
10^{-3}	9.8×10^{-13}	$0.292936 - 0.09766i$	10^{-3}	7.6×10^{-13}	$0.483644 - 0.0967588i$
10^{-4}	3.3×10^{-12}	$0.292936 - 0.09766i$	10^{-4}	1.2×10^{-11}	$0.483644 - 0.0967588i$
10^{-5}	2.7×10^{-11}	$0.292936 - 0.09766i$	10^{-5}	4.4×10^{-11}	$0.483644 - 0.0967588i$
10^{-6}	2.8×10^{-10}	$0.292936 - 0.09766i$	10^{-6}	3.7×10^{-10}	$0.483644 - 0.0967588i$
10^{-7}	–	–	10^{-7}	3.3×10^{-10}	–
10^{-8}	–	–	10^{-8}	–	–
10^{-9}	–	–	10^{-9}	–	–
10^{-10}	1.3×10^{-11}	$0.0833395 - 0.13145i$	10^{-10}	–	–

Table C.6: Residue value evolution for different values of the ϵ, in a Schwarzschild black hole for a gravitational perturbation, using the direct integration numerical method, for $l = 1$ (left) and $l = 2$ (right).

From these tables, it is clear that, in general, the optimal value for ϵ should be 10^{-3}. For both $l = 2$ and $l = 3$ for the gravitational case and $l = 1$ for the scalar case, the minimum value of residue is achieved for that value, showing some consistency in this parameter influence. For the smaller ϵ, some errors occurred in the code, which undermined its viability, but it still achieved some error-free results in some cases. However, from the values of ω, it is clear that these are not the best choices for this parameter.

C.3 ”Infinity” values analysis

For the last part of this section, we analyze how different values for infinity influence the results and their quality. For that, we try increments of 10, but always using half this distance for r_m. That way, we can

still compare these results with the rest, since there is coherence in the way that the quasinormal modes were calculated.

C.3.1 Gravitational perturbation

Infinity	Residue	Infinity	Residue
10	8.3×10^{-12}	10	1.8×10^{-11}
15	1.9×10^{-12}	15	4.4×10^{-13}
20	4.4×10^{-13}	20	6.8×10^{-13}
25	3.3×10^{-13}	25	1.6×10^{-13}
30	1.4×10^{-13}	30	5.0×10^{-12}
35	8.3×10^{-13}	35	9.5×10^{-13}
40	1.6×10^{-12}	40	1.7×10^{-12}

Table C.7: Residue value evolution for different values of "infinity", in a Schwarzschild black hole for a gravitational perturbation, using the direct integration numerical method, for $l = 2$ (left) and $l = 3$ (right).

C.3.2 Scalar perturbation

Infinity	Residue	ω	Infinity	Residue
10	3.0×10^{-11}	$0.292954 - 0.0976576i$	10	7.3×10^{-11}
15	4.3×10^{-11}	$0.292937 - 0.0976598i$	15	2.2×10^{-11}
20	3.3×10^{-12}	–	20	1.2×10^{-11}
25	5.6×10^{-12}	–	25	5.1×10^{-12}
30	1.4×10^{-11}	–	30	1.1×10^{-11}
35	2.4×10^{-11}	–	35	4.3×10^{-11}
40	1.6×10^{-10}	–	40	2.5×10^{-10}

Table C.8: Residue value evolution for different values of "infinity", in a Schwarzschild black hole for a gravitational perturbation, using the direct integration numerical method, for $l = 1$ (left) and $l = 2$ (right).

For this evolution, the majority of the values of ω did not change and remained equal to those obtained in tables (5.4,5.5,5.6). From the tables, one can see that the best values for the infinity distance are around 25 and 30. The values of the residue decrease significantly at first, reaching an optimal minimum, and then oscillating to larger values. However, for the matching point, we have always used half of the infinity distance, so some variations can occur, but that will be the most suitable interval for the integration.

D

State-of-the-art review and analysis

In this appendix, we reviewed the state-of-the-art work [38] addressing white hole quasinormal modes, to compare our results and proposals. To do that, we start with a brief and general view of this work and its arguments. We proceed to make a more thorough analysis, including some prior works and arguments used to obtain the results in this final paper.

D.1 Overview

This section was written prior to a thorough mathematical review of Sections II and III, as well as of some of the references important to this paper. Therefore, this subsection only presents the basic and most important points of the article, and can be used as the base for a more thorough and rigorous review. In the Introduction, we are presented with a general overview of the project, based on linear perturbations. Instead of Schwarzschild coordinates, it was decided to use Bondi-Sachs coordinates , which are based on outgoing null cones. The previous work to linearize Einstein equations using these coordinates, and test them in numerical relativity codes, was done in [39] and [40], which we will also review, as they are the base for this article. After obtaining the usual second-order ODE, it is said that the results obtained for the quasinormal modes are not the standard ones. This is unusual, since, from the reader's point of view, it seems to be difficult to connect the results obtained for the QNM with physical problem specifications such as boundary conditions or other properties. In the beginning, we are presented with two different hypersurfaces, with fields having different directions of propagation at the horizon and at infinity, for the black and white holes. However, it does not seem to be clear how these specific characteristics are integrated into solving the problem.

After carefully following the arguments and logic of Sections II and III, it seems that there is still an ambiguity regarding the boundary conditions, or other relations that would indicate for which object, region or hypersurface the QNM's are being calculated. Possibly, this problem may be answered in other papers cited, namely [39, 40]. Still in these sections, we find equation 5 of the paper, given by

$$x^3(1-2xM)\frac{d^2J_2}{dx^2}+2\frac{dJ_2}{dx}(2x^2+i\nu x-7x^3M)-2(x(l^2-l-2)/2+8Mx^2+i\nu)J_2=0. \tag{D.1}$$

This is the central piece in this problem, from where all the asymptotic solutions and numerical integrations are derived. Moving on to the results, a final estimate for the lowest mode is obtained with the value $\nu = 0.883 + i(0.641) + 0.003k$, with k being a complex number satisfying $|k| \leq 1$. There is also another quasinormal mode $\nu = 1.06 + i(0.63)$, that unfortunately is not investigated further. This section ends by stating that a quasinormal mode of a Schwarzschild BH is at $\nu = 0.37367 + i(0.08896)$, and that, when using this value in the code, it shows not to be a quasinormal mode of Eq. (D.1). These statements are mentioned in the conclusion, and, in order to avoid this discrepancy, the authors propose to interpret these QNMs as being those of a white hole. In addition, they highlight the crucial dependency of these

results on the validity of Eq. (D.1). There has been no subsequent, independent derivation, but it has been subject to consistency checks in [40], and for $M = 0$, has been tested as solutions in numecrical relativity codes based on the Bondi-Scahs metric [41, 42]. Nevertheless, the author's proposal does not seem to be totally rigorous, or even well-founded. The offered perspective seems to present a method for calculating QNMs without the clear specifications mentioned above. This method presents results that do not match the established QNM for the BH, nor is the established one compatible with Eq. (D.1). The WH proposal seems to be weak, since throughout the paper there does not seem to be any indication of boundary conditions that relate the result to this object.

D.2 Thorough Review

To start this review, we begin the analysis of [25] to understand the origin of equation (D.1).

D.2.1 Formalism: Bondi-Sachs metric

This formalism, used in the numerical evolution of Einstein's field equations, is characterized by using a family of outgoing null hypersurfaces. It uses u to label these hypersurfaces, x^A $(A = 2, 3)$ to label the the null rays, and r as a surface area coordinate along the rays. Therefore, using the coordinates $x^\alpha = (u, r, x^A)$, the Bondi-Sachs metric takes the form

$$ds^2 = -\left(e^{2\beta}\left(1+\frac{W}{r}\right) - r^2 h_{AB}U^A U^B\right)du^2 - 2e^{2\beta}dudr - 2r^2 h_{AB}U^B dudx^A + r^2 h_{AB}dx^A dx^B\,, \quad \text{(D.2)}$$

where $h^{AB}h_{BC} = \delta^A_C$ and $\det(h_{AB}) = \det(q_{AB})$, with q_{AB} the unit sphere metric. In this work, stereographic coordinates $x^A = (q, p)$ are used, for which the unit sphere metric is given by

$$q_{AB}dx^A dx^B = \frac{4}{P^2}(dq^2 + dp^2), \quad \text{with} \quad P = 1 + q^2 + p^2. \quad \text{(D.3)}$$

It also introduces a complex dyad q_A defined by

$$q^A = \frac{P}{2}(1, i)\,, \quad \text{(D.4)}$$

the quantities

$$J = h_{AB}q^A q^B/2 \qquad \text{and} \qquad U = U^A q_A \quad \text{(D.5)}$$

and, in addition, the complex differential eth operators $\eth$ and $\bar{\eth}$ [43]. Einstein's equations, written in the form $R_{\alpha\beta} = 8\pi\left(T_{\alpha\beta} - \frac{1}{2}g_{\alpha\beta}T\right)$, are then classified as: hypersurface equations with $R_{11}, q^A R_{1A}, h^{AB}R_{AB}$ forming a hierarchical set for β, U and W; evolution equation $q^A q^B R_{AB}$ for J; and constrains using $R_{0\alpha}$.

An evolution problem is normally formulated in the region of spacetime between a timelike or null worldtube Γ and future null infinity, with free initial data J given on u = 0. Boundary data for β, U, W, J, that satisfies the constraints, are required on Γ. In the case where the spacetime contains a single Schwarzschild black hole, Γ is usually taken to be the past event horizon $r = 2M$.

D.2.2 Spin-weighted spherical harmonics

This work uses spin-weighted spherical harmonics ${}_sY_{lm}$ [44, 45] and, as basis functions, the functions ${}_sZ_{lm}$ defined as

$$\begin{aligned}
{}_sZ_{lm} =& \frac{1}{\sqrt{2}}[{}_sY_{lm} + (-1)^m \times {}_s\, Y_{lm}] \quad \text{for} \quad m > 0\,, \\
{}_sZ_{lm} =& \frac{i}{\sqrt{2}}[(-1)^m \times {}_s\, Y_{lm} - {}_s\, Y_{lm}] \quad \text{for} \quad m < 0\,, \\
{}_sZ_{l0} =& {}_sZ_{l0}\,, \\
{}_0Z_{lm} =& Z_{lm}\,.
\end{aligned} \tag{D.6}$$

Some important properties of these functions are the facts that they are orthonormal and real. They also satisfy

$$\begin{aligned}
&\bar{\eth}\eth Z_{lm} = \eth\bar{\eth} Z_{lm} = L_2 Z_{lm}\,, \qquad \bar{\eth}\eth^2 Z_{lm} = (L_2 + 2)\eth Z_{lm}\,, \\
&\bar{\eth}^2\eth^2 Z_{lm} = \eth^2\bar{\eth}^2 = L_2(L_2 + 2) Z_{lm}\,,
\end{aligned} \tag{D.7}$$

with $L_2 = -l(l+1)$, and

$$\eth Z_{lm} = \sqrt{-L_2}_1 Z_{lm}; \qquad \eth^2 Z_{lm} =_2 Z_{lm}\sqrt{-l(l-1)L_2(l+2)}\,. \tag{D.8}$$

D.2.3 The linearized Einstein equations for the Bondi-Sachs metric

This article considers a matter distribution in the format of a thin, low-density shell around a Schwarzschild black hole or vacuum. The shell is taken to be spherical and placed at at $r =$constant, but with varying density ρ. The density and metric quantities are considered as being of first order, i.e $\rho, J, \beta, U, w = \mathcal{O}(\epsilon)$ with $W = -2M + w$ and M being the mass of the black hole. Ignoring terms of order $\mathcal{O}(\epsilon^2)$ and using

the ansatz above, the following forms for the hypersurface equations and evolution equations are found:

$$
\begin{aligned}
&R_{11} : \frac{1}{r}\partial_r\beta = 2\pi T_{11}\,,\\
&q^A R_{1A} : \frac{1}{2r}(4\eth\beta - 2r\eth(\partial_r\beta) + r\bar{\eth}(\partial_r J) + r^3\partial_r^2 U + 4r^2\partial_r U) = 8\pi q^A T_{1A}\,,\\
&h^{AB}R_{AB} : (4 - 2\eth\bar{\eth})\beta + \frac{1}{2}(\bar{\eth}^2 J + \eth^2\bar{J}) + \frac{1}{2r^2}\partial_r(r^4\eth\bar{U} + r^4\bar{\eth}U) - 2\partial_r w = 8\pi(h^{AB}T_{AB} - r^2 T)\,,\\
&q^A q^B R_{AB} : -2\eth^2\beta + \partial_r(r^2\eth U) - 2(r-M)\partial_r J - \left(1 - \frac{2M}{r}\right) r^2\partial_r^2 J + 2r\partial_u\partial_r(rJ) = 8\pi q^A q^B T_{AB}\,.
\end{aligned}
\tag{D.9}
$$

The constraint equations (needed only off the matter shell) are also evaluated, leading to (in the vacuum):

$$
\begin{aligned}
R_{00} : \frac{1}{2r^3}&(r(r-2M))\partial_r^2 w + \eth\bar{\eth}w + 2(r-2M)\eth\bar{\eth}\beta - Mr(\eth\bar{U} + \bar{\eth}U)\\
&- 4r(r-2M)\partial_u\beta - r^3\partial_u(\eth\bar{U} + \bar{\eth}U) + 2r\partial_u w) = 0\,,\\
R_{01} : \frac{1}{4r^2}&(2r\partial_r^2 w + 4\eth\bar{\eth}\beta - \partial_r(r^2\eth\bar{U} + r^2\bar{\eth}U)) = 0\,,\\
q^A R_{0A} : \frac{1}{4r^2}&(2r\eth\partial_r w - 2\eth w + 2r^2(r-2M)(4\partial_r U + r\partial_r^2 U) + 4r^2 U + r^2(\eth\bar{\eth}U - \eth^2\bar{U})\\
&+ 2r^2\bar{\eth}\partial_u J - 2r^4\partial_u\partial_r U - 4r^2\eth\partial_u\beta) = 0\,.
\end{aligned}
\tag{D.10}
$$

D.2.4 Eigenfunction decomposition

It is proposed that the metric quantities can be written as

$$
\begin{aligned}
J = J_0(r)\cos(\nu u)\eth^2 Z_{lm}\,, \qquad U = U_0(r)\cos(\nu u)\eth Z_{lm}\,,\\
\beta = \beta_0(r)\cos(\nu u)Z_{lm}\,, \qquad w = w_0(r)\cos(\nu u)Z_{lm}\,.
\end{aligned}
\tag{D.11}
$$

For these purposes, l, m, r_0 and ν are regarded as fixed. Later, the time variation will be expressed as $e^{i\nu u}$, but initially the dependence needs to be explicitly kept real. Choosing these basis functions as eigenfunctions of the relevant operators, one can apply the above ansatz to the equations in (D.9):

$$
\begin{aligned}
&\frac{1}{r}\partial_r\beta_0\cos(\nu u)Z_{lm} = 2\pi T_{11}\,,\\
&\frac{1}{2r}(4\beta_0 - 2r\partial_r\beta_0 + r(2+L_2)\partial_r J_0 + r^3\partial_r^2 U_0 + 4r^2\partial_r U_0)\cos(\nu u)\eth Z_{lm} = 8\pi q^A T_{1A}\,,\\
&\left(2(2-L_2)\beta_0 + (L_2(L_2+2))J_0 + \frac{1}{r^2}\partial_r(r^4 L_2 U_0) - 2\partial_r w_0\right)\cos(\nu u)Z_{lm} = 8\pi(h^{AB}T_{AB} - r^2 T)\,,\\
&\left(-2\beta_0 + \partial_r(r^2 U_0) - 2(r-M)\partial_r J_0 - \left(1 - \frac{2M}{r}\right) r^2\partial_r^2 J_0 - 2r\nu\frac{\sin(\nu u)}{\cos(\nu u)}(J_0 + r\partial_r J_0)\right)\cos(\nu u)\eth^2 Z_{lm} = 8\pi q^A q^B T_{AB}\,.
\end{aligned}
\tag{D.12}
$$

In this set, a possible error was detected in the second equation. After using the ansatz (D.11), we have arrived at $\partial_r J_0$ instead of just J_0, as in the paper. Given the following procedures, this change can implicate major differences in the final equation (D.1), and consequently in the final results. Nonetheless, we proceed with the review ignoring this error, keeping the derivative, to later see the impact that it might have.

D.2.5 Solution procedure

It is stated that the first equation in (D.12) shows that β_0 takes a constant value, β_{0+}, in the region $r > r_0$, and β_{0-} for $r < r_0$; we will assume $\beta_{0-} = 0$. Then it is argued that the second and the last equations in (D.12) constitute a coupled system of ordinary differential equations in $U_0(r)$ and $J_0(r)$. Once this system is solved, the third equation of (D.12) can be solved for $w_0(r)$. For simplicity, the case $l = 2$ (implying $L_2 = -6$) is considered. Taking $r > r_0$ and removing the common factors, we have

$$4\beta_{0+} - 4r\partial_r J_{0+} + r^3\partial_r^2 U_{0+} + 4r^2\partial_r U_{0+} = 0\,, \tag{D.13}$$

$$18\beta_0 + 24J_{0+} - \frac{6}{r^2}\partial_r(r^4 U_{0+}) - 2\partial_r w_{0+} = 0\,, \tag{D.14}$$

$$-2\beta_{0+} + 2rU_{0+} + r^2\partial_r U_{0+} - 2(r-M)\partial_r J_{0+} - r^2\left(1 - \frac{2M}{r}\right)\partial_r^2 J_{0+} + 2ri\nu(J_{0+} + r\partial_r J_{0+}) = 0\,. \tag{D.15}$$

The ansatz in (D.11) is then used in the constraints in (D.10) to simplify them. To obtain the central equation in (D.1), it is argued that one can manipulate the first and third equations (D.13), (D.15) to obtain it, taking into account that $J_2(x) = d^2 J_{0+}/dx^2$ and $x = 1/r$. The best way to do that is to take the U_{0+} terms in Eq. (D.13) and substitute in Eq. (D.15). One can first change variables for x, which makes equations (D.13), (D.15) take the following form:

$$4\beta_{0+} + 4x\partial_x J_{0+} + x\partial_x^2 U_{0+} - 2\partial_x U_{0+} = 0\,, \tag{D.16}$$

$$-2\beta_{0+} + \frac{2}{x}U_{0+} - \partial_x U_{0+} + \frac{2i\nu}{x}J_{0+} + (2Mx^2 - 2i\nu)\partial_x J_{0+} + (2Mx^3 - x^2)\partial_x^2 J_{0+} = 0\,. \tag{D.17}$$

However, after many attempts, using different methods, differentiating and substituting, in r or x coordinates, we could not reach equation (D.1). After careful review and consideration, taking into account the possible error earlier and the poor physical argumentation, as described in the overview, we decided to terminate the review of this work.